

## 5 Retrieval of sea ice drift in the Fram Strait based on data from Chinese satellite HaiYang (HY1-D)

Dunwang Lu<sup>1,2,3</sup>, Jianqiang Liu<sup>2,3</sup> (deceased), Lijian Shi<sup>2,3</sup>, Tao Zeng<sup>2,3</sup>, Bin Cheng<sup>4</sup>, Suhui Wu<sup>2,3</sup>, Manman Wang<sup>1,2,3</sup>

<sup>1</sup> National Marine Environmental Forecasting Center, Beijing 100081, China

10 <sup>2</sup> National Satellite Ocean Application Service, Beijing 100081, China

<sup>3</sup> Key Laboratory of Space Ocean Remote Sensing and Application, Ministry of Natural Resources, Beijing 100081, China

<sup>4</sup> Finnish Meteorological Institute, Helsinki 00101, Finland

Correspondence to: Lijian Shi (shilj@mail.nsoas.org.cn)

15 **Abstract.** Melting of sea ice in the Arctic has accelerated due to global warming. The Fram Strait (FS) serves as a crucial pathway for sea ice export from the Arctic to the North Atlantic Ocean. Monitoring sea ice drift (SID) in FS provides insight into how Arctic sea ice responds to the climate change. The SID has been retrieved from Sentinel-1 SAR, AVHRR, MODIS and AMSR-E, and further exploration is needed for the retrieval of SID using optical imagery. In this paper, we retrieve SID in the FS using Chinese HaiYang1-D (HY1-D) satellite equipped with the Coastal Zone Imager (CZI). Multi-template matching technique is employed to calculate cross-correlation, and subpixel estimation is used to locate displacement vectors from the cross-correlation matrix. The dataset covering March to May 2021 was divided into hourly and daily intervals for analysis, and validation was performed using Copernicus Marine Environment Monitoring Service (CMEMS) SAR-based product and IABP buoy. A comparison with the CMEMS SID product revealed a high correlation with the daily interval dataset; however, due to the spatial and temporal variability of sea ice motion, differences are observed with the hourly interval dataset. Additionally, validation with IABP buoy yielded a velocity bias of -0.005 m/s and RMSE of 0.031 m/s for the daily interval dataset, along with a flow direction bias of 0.002 rad and RMSE of 0.009 rad respectively. For the hourly interval dataset, the velocity bias was negligible (0 m/s), with a RMSE of 0.036 m/s, while the flow direction bias was 0.003 rad with a RMSE of 0.010 rad. In addition, during the validation with buoys, we found that the accuracy of retrieving the SID flow direction is distinctly interrelated with the sea ice displacement.

### 1 Introduction

30 The Arctic, as one of the three poles of the Earth (Li et al., 2020) that stores 101,000 km<sup>3</sup> of fresh water (Finnish Meteorological Institute et al., 2022), is an important part of the cryosphere and plays a prominent role in global water resources and atmospheric cycles. Since the beginning of the twenty-first century, global warming has profoundly affected human production and activities and has become a strong threat to the stability of the climate system (Cook et al., 2014). Under the effect of Arctic amplification (Serreze et al., 2009), Arctic quick warming accelerates the melting of polar sea ice, leads to thinner sea

Deleted: ocean

Deleted: s...into how Arctic sea ice responds to the climate change. The SID has been retrieving ...etrieved from Sentinel-1 SAR, AVHRR, MODIS and AMSR-E, and further exploration is needed for the retrieval of SID using optical imagery using optical data to retrieve SID still needs further exploration... In this paper, we retrieve SID in the FS using China's ...hinese HaiYang1-D (HY1-D) satellite equipped with the Coastal Zone Imager (CZI). Multi-template matching technique is employed to calculate cross-correlation, and subpixel estimation is used to locate displacement vectors from the cross-correlation matrix. The dataset covering March to May 2021 is...as divided into hourly and daily intervals analysis, and validation is ...as performed using Copernicus Marine Environment Monitoring Service (CMEMS) SAR-based product and IABP buoy measurements... A c...mparison with ...ith the SID product reveals ...evealed a high correlation at ...ith the daily level...nterval dataset; however, due to the spatial and temporal variability in ...f sea ice motion, differences are observed at ...ith the an ...ourly interval dataset resolution... Additionally, validation against ...ith IABP buoy data shows...ielded a a ...elocity bias bias...of -0.004 ...05 m/s and RMSE of 0.027 ...31 m/s forat...the day-...y level...nterval dataset, along with a ... flow direction bias of 0.057 ...02 rad and RMSE of 0.313 ...09 rad respectively; ... Fwhile at ...r the hour-...y level...nterval dataset, ...the velocity bias is ...as negligible (0 m/s),...with a an ...MSE value ...f 0.022 ...36 m/s;...

Deleted: similarly for flow direction bias which remains negligible.

Deleted: D...ring the validation against ...ith buoys, we find ...ound that the accuracy of retrieving the SID flow direction is highly ...

Deleted: n...important ...rominent role in global water resources and atmospheric cycles. Since the beginning of the twenty-first century, global warming has profoundly affected human production and activities and has become an important factor...strong threat toening...

130 ice and accelerates sea ice transport (Krumpfen et al., 2016; Maslanik et al., 2011). The acceleration of sea ice motion also indicates a reduction of the sea ice residence time in the Arctic (Sumata et al., 2023). Moreover, changes in sea ice feed back into the climate system, affecting energy transport (Dethloff et al., 2006; Döscher et al., 2014).

Sea ice drift (SID) is an important geophysical parameter to describe the dynamic of sea ice and the sea ice motion under the influence of winds, currents, and various external forces (gravity, Coriolis effect, etc.) (Encyclopedia of Ocean Sciences, 2022).

135 The primary SID circulation across the Arctic encompasses both the Beaufort Gyre (BG) and the Transpolar Drift (TPD) (Preller and Posey, 1989), and TPD transports large quantities of multiyear ice outward from the central Arctic toward the FS, Barents Sea and Baffin Bay (Colony and Thorndike, 1984; Martin and Augstein, 2000). The FS connects the Arctic and the North Atlantic (Sumata et al., 2022), and large quantities of sea ice are injected into the North Atlantic each year through the strait (Reimnitz et al., 1994). The long-term annual average ice outflow in the FS (1935-2014) is approximately 880,000 km<sup>3</sup>, accounting for 10% of the sea ice cover in the Arctic basin (Smedsrud et al., 2017) and the largest portion (90%) of the Arctic sea ice export volume (Sumata et al., 2022; Haine et al., 2015; Serreze et al., 2006). Sea ice, a mixture of ice and brine (Schwerdtfeger, 1963), which gradually disintegrates during outward transport in the FS. This process affects freshwater exchange and energy transport in the North Atlantic, which may alter the convective overturning of water masses and thermohaline circulation processes (Aagaard and Carmack, 1989). In addition, for shipping planning and scientific research,

140 the progression of polynyas and lead is heavily influenced by SID (Wagner et al., 2021). Therefore, observing SID in the FS is crucial to analyse the sea ice variation in the Arctic and the sea ice transport from the polar to sub-polar regions.

145 The development of satellites and remote sensing sensors promote satellite data as a prevailing trend in retrieving SID (Kwok, 2010). The SID retrieved from satellite-derived data possesses continuity in spatial and temporal, which helps researchers better evaluate the sea ice variation in the Arctic and provides a basis for climate forecasting and ship route planning. At present,

150 the primary data used in SID retrieval are radiometer, scatterometer, synthetic aperture radar (SAR) and optical imagery. SID products derived from radiometers and scatterometers inherently possess coarse spatial resolution owing to the characteristics of the sensors. Low resolution SID products exhibit large error on velocity in FS (Hwang, 2013). OSI SAF provides SID products retrieved from scatterometers and radiometers over the polar regions and its temporal coverage is from 2009 to now, however, the time interval of these products is greater than one day. Due to the complexity of sea ice dynamics, low temporal

155 resolution SID product may fail to depict the subdaily-scale variation of the sea ice motion. High spatiotemporal resolution SID products are valuable for capturing subtle SID patterns (Johansson and Berg, 2016). SAR image provides high spatial resolution, but radar backscatter is sensitive to the liquid water on sea ice surface, and the accuracy of retrieving SID during the melting season can be hampered (Stern and Moritz, 2002). This disadvantage constrains the application of SAR in retrieving SID. Optical imagery has been applied extensively in cryosphere observation. Many in orbit satellites equipped with optical

160 imagery and optical imagery have the advantages of wide swath and high resolution, which are beneficial for capturing the surface roughness and textural characteristics of sea ice. Optical imagery has the potential to retrieve SID in FS. While optical imagery has the advantages of high resolution and wide swath, this can also significantly increase the computational effort of the algorithm. To solve this problem, we applied the MCC (maximum cross-correlation) algorithm with improvements for SID

**Deleted:** Arctic quick warming accelerates the melting of polar sea ice, leading to accelerated sea ice break-up and sea ice transport... (Krumpfen et al., 2016; Maslanik et al., 2011). The acceleration of sea ice motion also indicates a decrease... reduction in... of the sea ice residence time of sea ice... in the Arctic (Sumata et al., 2023). Moreover, the

**Deleted:** Sea ice drift (SID) is an important geophysical parameter that describes the movements of sea ice, and it is the process of sea ice as it moves across the sea surface in response to winds, currents and other forces... (gravity, Coriolis effect, etc.) (Encyclopedia of Ocean Sciences, 2022). The primary SID circulation across the Arctic encompasses both the Beaufort Gyre (BG) and the Transpolar Drift (TPD) The large-scale SID over the Arctic consists of the Beaufort Gyre (BG) and the Transpolar Drift (TPD) ... ADDIN and the

**Deleted: -**

**Deleted:** is... a mixture of ice and brine (Schwerdtfeger, 1963), which gradually melts

**Deleted:** This

**Deleted:** understanding... bserve SID in the FS is crucial to recognizing... analyse how... the sea ice variation changes... in the Arctic and appreciating... the connection... sea ice transport from between... the polar regions and... o... sub-polar regions the outside world...

**Deleted:** With the launch of many remote sensing satellites and the development of remote sensing technology, remote sensing satellite data have become a major data source for SID retrieval... (Kwok, 2010). The SID retrieved from satellite-derived data possesses continuity in spatial and temporal. Satellite data can be retrieved to obtain a spatially and temporally continuous sea ice drift field... which helps researchers to... better evaluate the sea ice variation in the Arctic and provides a basis for climate forecasting and ship route planning. At present, the primary data used in SID retrieval are radiometers... scatterometers... synthetic aperture radar (SAR) and optical imagers... SID Products... products derived from radiometers and scatterometers inherently possess coarse spatial resolution owing to the characteristics of the sensors. based on radiometers and scatterometers often yield lower resolution due to the inherent characteristics of the sensors... Low resolution SID products... exhibit large errors... on ice drift speed... elocity in the... S region

**Deleted:** OSI SAF scatterometer and radiometer based SID products are available for many years over FS region... however, the products tend to have... ime intervals

**Deleted:** provide accurate sea ice drift patterns... High spatiotemporal resolution SID products are highly... valuable for capturing subtle SID sea ice drift... atterns (Johansson and Berg, 2016). SAR images... provides high spatial resolution, but radar backscatter is sensitive to the liquid water on the... sea ice surface

**Deleted:** optical imagery can... accurately... apturing... the surface roughness and texture... extural characteristics of sea ice. Thus, ...

**Deleted:** optical remote sensing data... have... as the potential to retrieve SID in the... FS (Petrou and Tian, 2017)... While optical imagery has the advantages of high resolution and wide swath, this can also significantly increase the computational effort of the algorithms... To solve this problem, our study

305 retrieval. The MCC has been widely used in retrieving SID with radiometer and scatterometer, as well as with SAR (Girard-Ardhuin and Ezraty, 2012; Hollands and Dierking, 2011). However, when it comes to utilizing optical imagery for SID retrieval, many researchers tend to use different algorithms instead of the MCC. [Petrou et al.] designed an algorithm based on optical flow to retrieve SID from MODIS (Petrou and Tian, 2017). However, due to the absence of buoy, in their study area, the accuracy of their algorithm is unevaluated. [Lopez-Acosta et al.] developed a complex ice tracking algorithm specifically designed for retrieving SID in FS, but requiring multiple MODIS images to generate a complete SID field (Lopez-Acosta et al., 2019). [Fang et al.] discussed the potential of feature tracking with MODIS images for SID retrieval. The accuracy of their result is promising (Fang et al., 2023), but the spatial coverage needs to be further improved. [Wang et al.] designed an ice tracking algorithm to retrieve SID in the marginal ice zone (MIZ), but the algorithm cannot produce an intact SID field (Wang et al., 2021). The European Organization for the Exploitation of Meteorological Satellites (EUMETSAT) uses the MCC algorithm to retrieve SID from AVHRR with a spatial resolution of 20 km and a temporal resolution of 1 day (Dybkjaer, 2018). However, it has been found that the accuracy of the SID product retrieved from AVHRR presents low accuracy in East Greenland, with the Mean Absolute Error (MAE) of velocity reaching 10.40 km/day, which is even lower than that of the SID products retrieved from radiometer and scatterometer (Wang et al., 2022). In our study, we applied multi-template matching combined with a subpixel estimation for SID retrieval. The method of multi-template matching achieves a balance between computational efficiency and accuracy, and the subpixel estimation further improves the accuracy of the retrieval results while saving computational resources. We believe that the MCC algorithm with improvements can be utilized for retrieving SID effectively from optical imagery.

310

315

320 This paper focuses on designing an improved MCC algorithm using the Coastal Zone Imager (CZI) of Haiyang-1D (HY-1D) data to retrieve SID in the FS. Moreover, the retrieved results are evaluated via comparison with SAR-based SID products released by CMEMS and IABP buoy data. For sea ice motion, the average velocity of the sea ice motion in Arctic is 0.02 m/s (Colony and Thorndike, 1984), and the maximum velocity of the sea ice in the FS is 0.64 m/s (Lei et al., 2016). The multiyear ice (MYI) drifts from the Arctic basin and crushes in the central part of strait, which results in the fragmented ice in the southern part of the FS and along the eastern coast of Greenland. The fragmented ice drifts at a faster velocity near the FS compared to sea ice within the Arctic Basin. The sea ice characteristics described above increase the difficulty of retrieving SID in FS.

325

330 This paper is structured as follows. Section II describes the data used in this study, including the CZI image, CMEMS SID products and IABP buoy. Section III details the algorithm used to retrieve SID. Section IV compares the results with CMEMS SID products and buoy data for validation. Section V discusses the retrieved results. Finally, concluding remarks are provided in Section VI.

**Deleted:** employed ...sed in retrieving SID with radiometers...and scatterometers

**Deleted:** images...for SID retrieval, many researchers tend to choose ...se different algorithms in addition to...instead of the MCC. [Petrou et al.] designed an algorithm based on optical flow to retrieve SID from MODIS (Petrou and Tian, 2017). Nevertheless...owever, due to the absence of buoys...in their study area, the accuracy of their algorithm is unevaluated. [Lopez-Acosta et al.] developed a complex ice tracking algorithm specifically designed for retrieving SID in the ...S region...but requiring multiple MODIS images to generate a complete sea ice drift...ID field (Lopez-Acosta et al., 2019). [Fang et al.] discussed the potential of feature tracking algorithms in enhancing...ith MODIS images for SID retrieval. The accuracy of their result is promising...cellent... but the defect in which feature tracking produce vectors that are widely distributed and uniform in the SID field still unsolved ... ADDIN ZOTERO\_ITEM CSL\_CITATION needs to be further improved. [Wang et al.] also ...signed an ice tracking algorithm to retrieve SID in the marginal ice zone (MIZ), but the algorithm cannot produce an intact SID field (Wang et al., 2021). The European Organization for the Exploitation of Meteorological Satellites (EUMETSAT) uses the MCC algorithm to retrieve SID from AVHRR with a ... spatial resolution of 20 km and a ... temporal resolution of 1 day (Dybkjaer, 2018). However, it has been found that the accuracy of the SID product retrieved from AVHRR presents low accuracy in East Greenland...with thea...Mean Absolute Error (MAE) in speeds...f velocity reaching 10.40 km/day, which is even lower than that of the SID products retrieved fromof...radiometer and scatterometer (Wang et al., 2022). In our study, we apply ...plied multi-template matching combined with a subpixel estimation algorithm ...or SID retrieval. The method of multi-template matching achieves a balance between computational efficiency and accuracy, and the subpixel estimation further improves the accuracy of the retrieval results while saving some...computational resources... We believe that the using ...CC algorithm with improvements can be utilized for retrieving SID effectively from optical imagery, the MCC algorithm can be effectively utilized for retrieving SID from optical images.

**Deleted:** by comparing them ...ith SAR-based SID products released by CMEMS and IABP buoy data. As f...or sea sea ...ce motion, the average velocity of the sea ice motion in Arctic is 0.02 m/s (Colony and Thorndike, 1984), and the maximum velocity of the sea ice in the FS is 0.64 m/s (Lei et al., 2016)as the main export of sea ice from the Arctic, the sea ice in the FS can achieve a maximum velocity of 0.5 m/s (Qiu and Li, 2022), which makes retrieving SID of the area more sophisticated... The multiyear ice (MYI) drifts from the Arctic basin and crushes in the central part of strait, which results in the fragmented ice in the southern part of the FS and along the eastern coast of Greenland.Multiyear ice (MYI) drift from the Arctic basin is intensely fragmented in the central strait by TPD and multiple external forces, which makes the sea ice in the southern part of the FS and on the east coast of Greenland exist as drift ice...The fragmenteddrift...ice drifts at a faster rate ...elocity near the FS compared to sea ice within the Arctic Basin. The sea ice characteristics described above increase the difficulty of

**Deleted:** The ...his paper is structured as follows. Section II describes the data used in this study, including the CZI data...mage, CMEMS SID products and IABP buoy data... Section III details the algorithms...used to retrieve SID in our study

## 2 Data

### 2.1 HY-1D CZI data

480 Haiyang-1D (HY-1D) satellite was launched in 11 June 2020. The satellite is equipped with the Chinese Ocean Color and Temperature Scanner (COCTS), CZI, Ultraviolet Image (UVI), Satellite Calibration Spectrum, and Automatic Identification System. The revisit period of the CZI is three days, the resolution of the CZI image is 50 m, and the swath of the CZI image is nearly 950 km. CZI possesses four bands (VIR and NIR), as shown in Table 1. The wide swath and high spatial resolution of CZI imagery make it suitable for the sea ice motion observation in FS.

485 Since the launch of China's first ocean satellite in 2002, concerted efforts have been undertaken to institute a comprehensive global operational ocean satellite observation system. Currently, the observation system consists of 10 satellites, which include three series: ocean color series satellites (HY-1), ocean dynamic environment series satellites (HY-2), and ocean surveillance and monitoring series satellites (HY-3) (Zeng et al., 2023). In this paper, SID retrieval is performed using the LIC data which is processed with radiometric calibration and geographic projection. Before retrieving, the CZI images are resampled to 300 m considering the algorithm's computational efficiency and the spatial resolution of the result.

490 Table 1: Information on the HY-1D CZI data.

Band	Wavelength ( $\mu\text{m}$ )	Band name
1	0.42-0.50	Blue
2	0.52-0.60	Green
3	0.61-0.69	Red
4	0.76-0.89	Near Infrared

495 In the FS, the climate condition is harsh and sea ice changes rapidly in response to wind (Tsukernik et al., 2010), which is a potentially hazardous factor for shipping and scientific expeditions. Achieving timely and accurate monitoring of SID is a crucial goal. The CZI image has the high spatial resolution and wide swath for providing accurate monitoring of the SID. In our study, 111 CZI images from March to May 2021 were used to produce the intersection region (as shown in Fig. 1(a)) for the dataset, and 48 pairs of images were eventually produced for SID retrieval. Furthermore, to explore the influence of the image time interval on retrieval SID, the 48 pairs of image datasets are divided into 16 pairs of hours-level (less than 6 hours) dataset, and 32 pairs of day-level (approximately 24 hours) dataset. Fig. 1(b) shows the time intervals of image pairs, and Fig. 1(c) plots the outer frame lines of the image pairs, where the white borders are the locations of the image pairs with hours-level interval, and the darker blue borders are the locations of the image pairs with day-level interval.

Deleted: HY-1D

Deleted: The wide swath and high resolution of CZI give us an opportunity to understand the sea ice motion in the FS in detail.

Deleted: from CZI.

Deleted: T

Deleted: for

Deleted: s

Deleted: on

Deleted:

Deleted: For the Arctic region

Deleted: where

Deleted: s

Deleted: are

Deleted: shifts in ocean currents and

Deleted: s

Deleted: this

Deleted: of polar research

Deleted: are

Deleted: calculate

Deleted: to produce the

Deleted: forty-eight

Deleted: are

Deleted: sea ice

Deleted: s

Deleted: s

Deleted: histogram

Deleted: at the

Deleted: at

Deleted: the

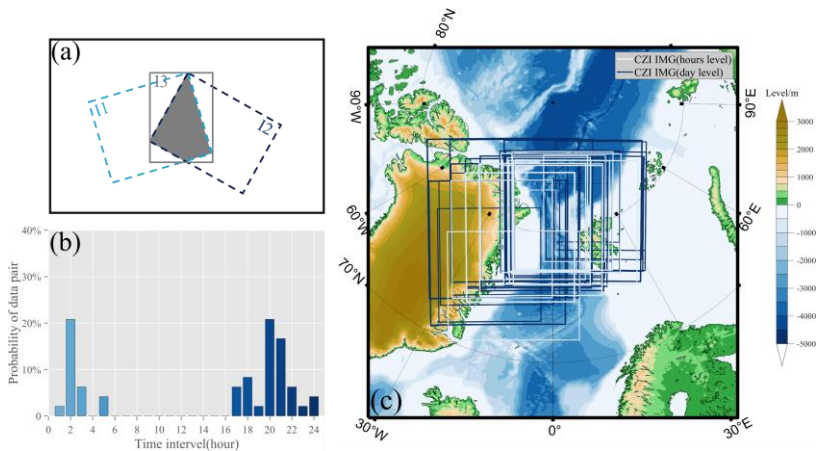


Figure 1: An illustration showing the creation of the dataset using CZI images (a), The time interval histogram of the dataset (b) and the location of image pairs (c).

## 2.2 CMEMS SID product

As the CZI images possess a high spatial resolution, the SID products retrieved from the scatterometer and radiometer are not comparable for validation. Thus, the SAR-based SID product is chosen for comparison. The Global Ocean-High Resolution SAR Sea Ice Drift is a polar near real-time gridded sea ice drift product produced by the National Space Institute at the Technical University of Denmark (DTU space) (European Union-Copernicus Marine Service, 2015). The data is released by the Copernicus Marine Environment Monitoring Service (CMEMS) and distributed on the website of Copernicus Marine Service. The composite product is updated every 12 hours covering 24 hours. Thus, two kinds of product are provided, with a nominal time intervals of 0:00 to 0:00 and 12:00 to 12:00, respectively. The grid resolution of the product is 10 km, and the product is available from both Arctic Ocean and South Ocean (Pedersen et al., 2015). The product has been validated using Woods Hole ice tethered profilers (ITPs). For the validation of 2021, the number of matched pair is 29180, the correlation coefficient between the product and ITP buoys is 0.99, and RMSD of dx and dy is 362.32 m (0.0042 m/s) and 339.81 m (0.0039 m/s), the BIAS of dx and dy is 4.64 m and 17.29 m and the BIAS of velocity is negligible (~0 m/s). The validation is performed with the 24-hour mean composite product. (European Union-Copernicus Marine Service, 2015). Sea ice motion changes rapidly in the FS, and SID results retrieved from images at different times is incompatible. Therefore, the CMEMS SID product which has the most temporal overlap with CZI images is chosen for comparison. Additionally, due to the disparity in spatial resolution, we resampled the retrieved SID to the resolution of the CMEMS SID product by linear interpolation.

Deleted: Example

Deleted: ing

Deleted: a clipped image

Deleted: ,

Deleted: es

Deleted: we choose

Deleted: are

Deleted: website

Deleted: The nominal time interval of each product is 24 hours.

Deleted: the product includes the North Pole and South Pole

Deleted: routinely every three months

Deleted: drift

Deleted: retrieving

Deleted: at

Deleted: The CMEMS product with more overlap with the time range of CZI images is chosen for comparison.

## 565 2.3 IABP buoys

570 GPS position data from buoys are the most credible data for the retrieved SID validation. The International Arctic Buoy Programme (IABP) has deployed a network of drifting buoys in the Arctic to provide data for scientific research (Rigor et al., 2008). IABP has collected more than 500 months of data from more than 500 buoys deployed in the Arctic. Buoy data collected from IABP are an essential component of Arctic scientific data. These data have been used to validate retrieved SID (Hakkinen et al., 2008; Fang et al., 2023). The drift trajectories of the 50 buoys used in our study are shown in Fig. 2 and these drift trajectories consist of consecutive GPS points. Among the buoys used for validation, 31 buoys from MOSAiC were included. The GPS position of MOSAiC buoy has an accuracy of  $\pm 2.5$  m (Qiu and Li, 2022) and the IABP buoy has an accuracy of approximately 300 m (Haarpaintner, 2006). We set a minimal distance of 4 km to search the buoys for validation. Because some of the buoys were deployed in the vicinity, we used the average of them to validate the result. Ultimately, 206 matched drift vectors were produced for validation.

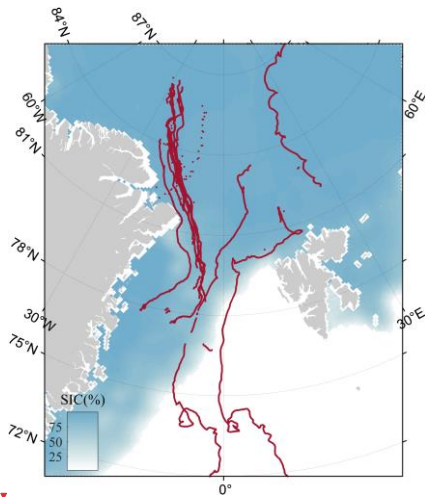


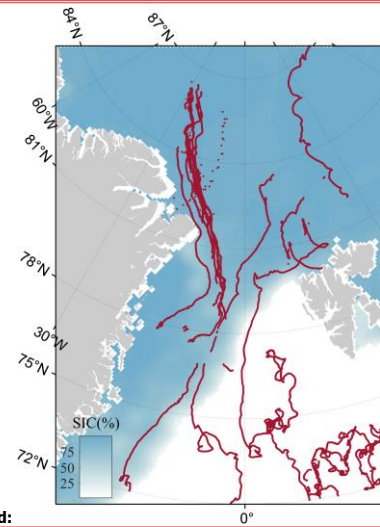
Figure 2: Drifting trajectories of 50 IABP buoys from March to May 2021, SIC (sea ice concentration).

### 3 Improved SID retrieval method in the Fram Strait

580 The flowchart of our study is shown in Fig. 3. We choose same orbit images of different moments to calculate the intersection and the intersection area is clipped to generate dataset. Data enhancement in preprocessing is used to distinguish between sea ice and seawater and highlight the textural details of the sea ice. Data enhancement is practical for retrieving SID using optical

**Deleted:** source ...or the retrieved SID's...validation. The International Arctic Buoy Programme (IABP) has deployed a network of drifting buoys in the Arctic to provide data for scientific research (Rigor et al., 2008). IABP has collected over ...ore than 500 months of data from over ...ore than 500 buoys deployed in the Arctic. Buoy data collected from IABP are an essential component of Arctic scientific data. These data have been widely ...sed to validate retrieved SID (Hakkinen et al., 2008; Fang et al., 2023). The drift trajectories of the 69 ...0 buoys in this paper...sed in our study are shown in Fig. 2 and these drift trajectories consist of consecutive GPS points. Among of ...he buoys used for validation, 33 ...1 buoys from MOSAiC are ...ere included. The GPS position of MOSAiC buoy has an accuracy of  $\pm 2.5$  m (Qiu and Li, 2022) and the IABP buoy has an accuracy of approximately 300 m (Haarpaintner, 2006).

**Deleted:** Based on the buoys data, 344 matched drift vectors were produced for the retrieved SID's validation.



**Deleted:**

**Deleted:** The d...rifting trajectories of 69

**Deleted:** Retrieval ...etrieval Method

**Deleted:** data processing ...lowchart of this paper...ur study is shown in Fig. 3. We choose same orbit images of different moments to calculate the intersection and Although the CZI image has a large swath, a single image can only partially cover the FS. Therefore, mosaicking of the images is necessary. After mosaicking, ...he intersection area is clipped to generate a set of image pairs...ataset. Data enhancement in preprocessing is used to increase ...istinguishthe distinction...between sea ice and seawater in the image...and...highlighting...the textural details of the sea ice. Data enhancement is indispensable

imagery (Fang et al., 2023; Lopez-Acosta et al., 2019; Yan et al., 2023). After preprocessing, the sea ice displacement will be retrieved via multi-template matching and subpixel estimation. Since the optical images are susceptible to various factors, such as cloud and the angle of incidence of the light (Stow et al., 2004), the SID contains noise and low-quality result. We designed the quality control session to remove the low-quality result and noise from the SID. The penultimate step involves smoothing and filling to derive an intact SID field. Finally, we validate the results using buoys and the CMEEMS SID product

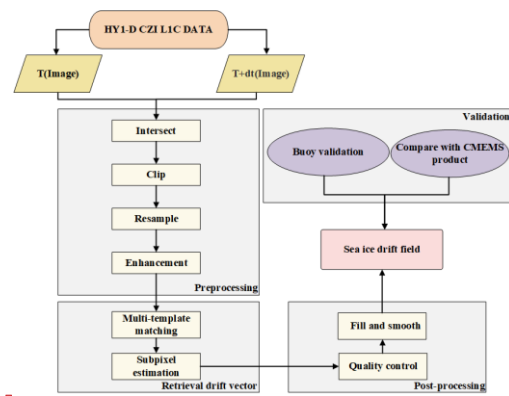


Figure 3: Flow chart of sea ice drift retrieval.

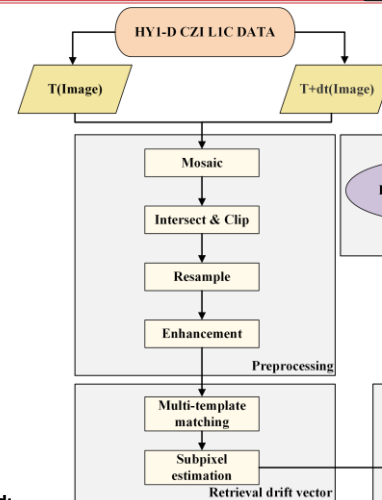
### 3.1 Data enhancement

Before preprocessing, the resampled image radiance values are converted to grayscale (0-255). Then, the data of different bands are stretched logarithmically. After reviewing study in which optical imagery was used to retrieve SID (Fang et al., 2023), we selected the average of the bands 2, 3, and 4 as the input data. Finally, histogram equalization and edge detection are applied to the image. The process and effect of data enhancement are explicitly described as follows.

In the polar regions, the lighting conditions are complex, and some images are captured at slight solar zenith angle (Stow et al., 2004). These disadvantages could lead to an uneven spatial distribution of image gray values, which affects the retrieval of SID. Logarithmic stretching is an image grayscale transformation that expands the low gray value portion and compresses the high gray value portion (Lupton et al., 2004). Equation (1) is the formula for logarithmic stretching, where  $r$  is the gray value of the image and  $c$  is the base. The larger the base is, the stronger the emphasis on the lower gray portions and the stronger the compression of the higher gray portions. As shown in Fig. 4(a) and (b), logarithmic stretching improves the uneven lighting and enhances the sea ice texture.

$$T(r) = c * \log(1 + r), \quad (1)$$

**Deleted:** optical images. Some research has applied data enhancement in preprocessing with optical images... (Fang et al., 2023; Lopez-Acosta et al., 2019; Yan et al., 2023). The data enhancement process can aid our algorithm, based on MCC, to retrieve SID more precisely. ... After preprocessing, the sea ice displacement will be retrieved by ... via multi-template matching and subpixel estimation. Since the optical images are susceptible to some ... various factors, such as clouds ... and the angle of incidence of the light (Stow et al., 2004), the SID contains noise and low-quality result, field with noise and low cross-correlation exist in the results, and ... Ww ... designed a ... the quality control session to remove the low-quality data ... result and noise from the results ... ID. The penultimate step is ... involves smoothing and filling to derive an SID field. Finally, we validate the results with ... using buoys and the CMEEMS SID products



**Deleted:** logarithmically ... stretched logarithmically separately. ... After reviewing study in which optical imagery investigating studies that used optical sensors ... was used to retrieve SID (Fang et al., 2023), we selected the average of the bands 2, 3, ... and 4 as the input data for the algorithm. ... Finally, histogram equalization and edge detection applied to the images

**Deleted:** with a

**Deleted:** is ... the stronger the the ... emphasis is ... on the lower gray portions and the stronger the compression of the higher gray portions is ... As shown in Fig. 4(a) and (b), applying ... logarithmic stretching to the image corrects ... improves the uneven lighting and enhances the sea ice detail in darker areas

In addition to logarithmic stretching, histogram equalization (HE) is also useful for adjusting the grayscale distribution of image (Krutsch and Tenorio, 2011). The adaptive histogram equalization (AHE) algorithm is a variant of histogram equalization (Pizer et al., 1987). The contrast is changed by calculating the local histogram of the image and then redistributing the value. The algorithm is an improvement over the traditional HE, but the disadvantage of AHE is that it introduces noise during grayscale stretching. Currently, contrast limited adaptive histogram equalization (CLAHE) has improved upon AHE (Zuiderveld, 1994). Therefore, we chose CLAHE to redistribute the gray values. The image histograms during grayscale transformation are shown in Fig. 4(d). Logarithmic stretching improves the gray value of the image (Fig. 4(b)), and CLAHE enhances the texture and gap features in high sea ice concentration regions (Fig. 4(c)). Cloud can lead to loss of contrast and diminished textural detail, affecting the quality of the result. Edge detection, the detection and characterization of significant intensity changes (Torre and Poggio, 1986), is valuable for reinforcing the texture differences between cloud and sea ice. In our study, Sobel edge detection is applied to enhance the texture, and we find that edge detection can also neutralize some disadvantageous effect of cloud. We will describe this aspect thoroughly in the discussion section.

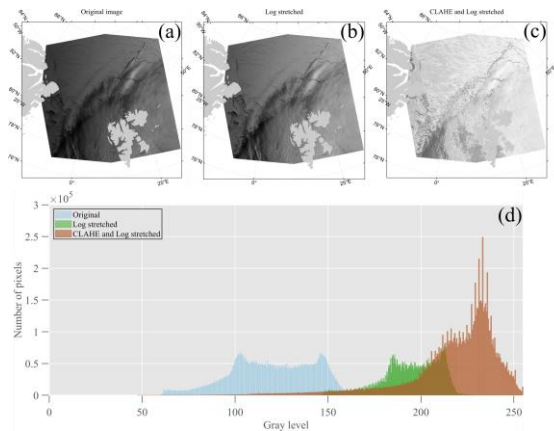


Figure 4: An example of a CZI image (average of bands 2, 3 and 4) before and after data enhancement and its grayscale histogram. (a) is the original image and the color of its histogram is light blue, (b) is the image after logarithmic stretching and the color of its histogram is green, (c) is the image after logarithmic stretching and CLAHE and the color of its histogram is brown, and (d) is the grayscale histogram of the above images. The date of the image is 07 April 2021, 07:16:35 LT.

### 3.2 Sea ice drift retrieval

#### 3.2.1 Multi-template matching

The traditional template matching requires searching in the vicinity of template, to determine the location with the largest correlation coefficient, which consumes considerable time. Multi-template matching is performed with different template sizes,

- Deleted: a common method
- Deleted: to
- Deleted: s
- Deleted: It changes t
- Deleted: image
- Deleted: This
- Deleted: method
- Deleted: over
- Deleted: ;
- Deleted: t
- Deleted: , in this study
- Deleted: of the image
- Deleted: change in the
- Deleted: is
- Deleted: of sea ice
- Deleted: dense
- Deleted:
- Deleted: cover
- Deleted: ould
- Deleted: a
- Deleted: e
- Deleted: retrieval
- Deleted: is a method of image enhancement in computer vision (...)
- Deleted: of sea ice
- Deleted: remove
- Deleted: of the
- Deleted: s
- Deleted: thin
- Deleted: s
- Deleted: in more detail
- Deleted: the
- Deleted: ,
- Deleted: their
- Deleted: retrieval of SID
- Deleted: a range of images
- Deleted: and this step could
- Deleted: a
- Deleted: amount of
- Deleted: can be
- Deleted: at

ranging from coarse resolution to fine resolution, reducing calculation time while ensuring accuracy (Wang et al., 2008). As shown in Fig. 5, the time cost of multi-template matching for the 48 datasets is less than 150 s, and the average number of image pixels uses for the retrieval is 5,208,298. This indicates that multi-template matching has high computational efficiency for wide-swath images. In addition, cross-correlation calculation is required during template matching, and the calculation is slow in the spatial domain (Thielicke and Stambhuis, 2014) and cannot yield a correlation matrix with equal size to the template.

Therefore, we calculate the correlation in the frequency domain using Fast Fourier Transform (FFT).

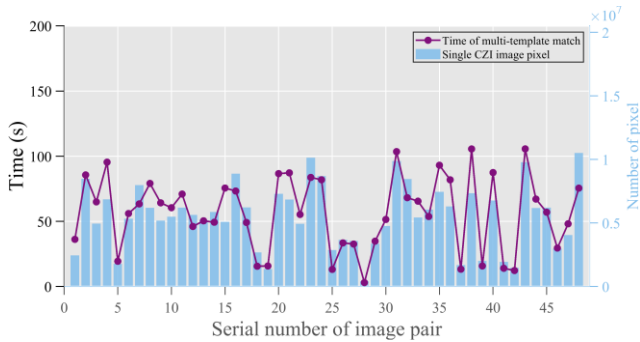


Figure 5: Relationship between multi-template matching time and image size.

### 3.2.2 Subpixel estimation

Identifying the peak of the correlation coefficient is an essential factor for improving the accuracy of retrieval. The integer displacements of the two templates can be determined directly from the peak positions of the correlation matrix. However, this approach introduces quantization error, and the difference of the minimum displacements will be multiples of the image resolution (Lavergne et al., 2010). To address this issue, subpixel precision refinement of the peak position with the biquadratic surface fitting method has been proposed to mitigate quantization errors (Kwok et al., 1998). Subpixel estimation could result in considerable computational costs when using sophisticated fitting (Hollands and Dierking, 2011). Therefore, for our study, we have opted for simple Gaussian fitting since this approach strikes a balance between computational efficiency and accuracy (Thielicke and Stambhuis, 2014).

### 3.3 Quality control

The retrieved SID obtained through multi-template matching and subpixel estimation is presented in Fig. 6(a). However, due to the influence of cloud and seawater, certain areas of SID have low confidence level. The algorithm may extract erroneous SID vectors, and it is necessary to filter those erroneous vectors. Therefore, we employ a series of methods to control the quality of the SID. By applying quality control, consistency within the SID is ensured while eliminating erroneous drift vectors. Subsequent sections provide detailed descriptions of the quality control procedures.

**Deleted:** to ...duce...ng calculation time while ensuring accuracy (Wang et al., 2008). As multi-template matching accounts for the efficiency of the calculation while guaranteeing accuracy, this method is chosen in the study to retrieve SID. ...s shown in Fig. 5, the time cost of multi-template matching for the 48 data pairs...ets designed in this study ...s under ...ess than 150 s, and the average number of image pixels uses for the retrieval in the retrieved images ...s 5,208,298 pixels... This result ...ndicates that multi-template matching has ...asa...high computational efficiency for wide-swath images... In addition, cross-correlation calculations...is are ...equred during template matching, and the calculations...is are ...low in the spatial domain (Thielicke and Stambhuis, 2014) in the spatial domain ...nd cannot yield a correlation matrix of roughly...ith equal size to the template. Therefore, we calculate the correlation in the frequency domain using Fast Fourier Transform (FFT). to save computational resources.

**Deleted:** R...lationship between multi-template matching time cost...

**Deleted:** The method of ...dentifyinglocating...the maximum ...eak of the correlation coefficient is an essential factor in ensuring...or improving the accuracy of the MCC...etrieval. The integer displacements of the two templates can be determined directly from the peak positions of the correlation matrix. However, this approach may ...ntroduces quantization errors... and the differenc...

**Formatted:** Font: (Default) Times New Roman, (Asian) Times New Roman

**Deleted:** address...this issue, subpixel precision refinement of the peak positions...with the biquadratic surface fitting method has been proposed to mitigate quantization errors (Kwok et al., 1998), but [Thomas et al.] mentions in their research that...Ss...bpixel estimations...could result in considerable computational costs when using sophisticated fitting (Hollands and Dierking, 2011). Therefore, for our study, we have opted for simple Gaussian fitting as a method for subpixel estimation ...ince it

**Deleted:** After performing...hrough multi-template matching and subpixel estimation, the retrieved SID field...is presented in Fig. 6(a). However, due to the influence of clouds...and seawater, certain areas of the obtained displacement field exhibit a...ID have low confidence level. The MCC ...lgorithm may erroneously...extract erroneous SID vectors, and it is necessary to filter those erroneous vectors (Haarpainter, 2006; Lavergne et al., 2010)... Therefore, we employ a series of methods to ensure

**Deleted:** displacement field...ID. By applying these...quality control measures... consistency within the displacement field...ID is ensured while eliminating erroneous drift fields ...ectorspresent in open water regions... Subsequent sections provide detailed of these...quality control procedures methods

### 3.3.1 Cross-correlation value and its derived parameters filter

The magnitude of the cross-correlation ( $R$ ) in the MCC serves as an indicator of result quality (Haarpaintner, 2006). It represents the correlation between two templates, making it an effective parameter for the initial quality control. Additionally, we employ two parameters derived from the cross-correlation matrix to further control the quality. In the selection of peak, incorrect peaks which are observed near the peak can be labeled as subpeaks. The ratio of peak to subpeak was used to measure of the 'uniqueness' of the real peak. Furthermore, comparing the average of the correlation coefficient matrix with the peak provides a measure of the signal-to-noise level of the peaks. Two parameters, the peak mean ratio (PMR) (Eq. 2) and the peak second ratio (PSR) (Eq. 3) (Dybkjaer, 2018; Van Wyk de Vries and Wickert, 2021), are used to measure the quality of the result.

$$PMR = \frac{C_{peak}}{\text{mean}(\text{abs}(C_{all-corr}))} \quad (2)$$

$$PSR = \frac{C_{peak}}{C_{subpeak}} \quad (3)$$

In the above equation,  $C_{peak}$  is the peak of cross-correlation,  $C_{all-corr}$  is the cross-correlation matrix, and  $C_{subpeak}$  is the second peak of cross-correlation. Fig. 6(c) shows the result obtained using a neighborhood filter and co-filtering with the cross-correlation value and its derived parameters filter. Compared to Fig. 6(b), which solely employs the neighborhood filter, incorporating the cross-correlation and derived parameters filter effectively eliminates erroneous outcomes within open water regions.

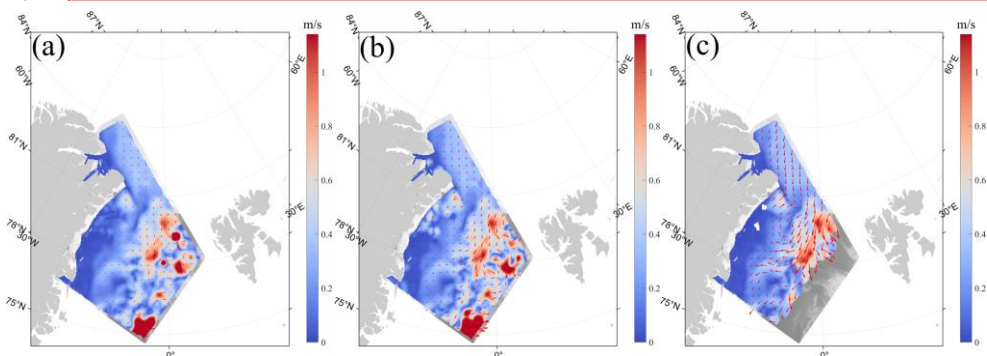


Figure 6: An example of quality control applied to the retrieved SID. (a: SID with no quality control, b: SID after neighborhood filter (only), c: SID after using neighborhood filter and cross-correlation value and its derived parameters filter).

- Deleted: method
- Deleted: suitable
- Deleted: result
- Deleted: ensure
- Deleted: result
- Deleted: s
- Deleted: s
- Deleted: and
- Deleted: also
- Deleted: Measuring t
- Deleted: s
- Deleted: s
- Deleted: provides a
- Deleted: mean
- Deleted: s
- Deleted: PMR (
- Deleted: )
- Deleted: PSR (
- Deleted: )
- Deleted: sum of the
- Deleted: value
- Deleted: s
- Deleted:

- Deleted: sea ice drift retrieval
- Formatted: Font: (Default) Times New Roman, (Asian) Times New Roman

### 3.3.2 Neighborhood filter

The neighborhood filter is commonly employed for postprocessing retrieved SID data by removing abrupt values indicative of incidental anomalous drifts that deviate from continuous sea ice movement patterns (Hyun and Kim, 2017; Girard-Ardhuin and Ezraty, 2012). In our study, two window sizes are designed for neighborhood filter. Fig. 6(b) shows the results of using the neighborhood filter only. Compared to Fig. 6(a), the neighborhood filtering removes the regions (upper part of the image) with significant velocity differences in the SID, but only using only the neighborhood filter is not incomplete. Combining the cross-correlation value and its derived parameters filter is necessary to comprehensively control the quality of the result.

### 3.4 Fill and smooth

The utilization of correlation coefficient and its derived parameters filter, and neighborhood filter, introduces missing values to the results. Given that the sea ice is spatially distributed continuously, adjacent values are employed to fill in these gaps and smoothen the outcomes during the final step of retrieval.

## 4 Results and validation

In this study, SID in FS is retrieved from the CZI images with a resolution of approximately 4 km. The results are categorized into day-level and hours-level datasets based on the time interval of images and compared with the IABP buoy and the CMEMS SID product.

### 4.1 Comparison of results with CMEMS products

#### 4.1.1 SID with day-level time intervals

Higher-resolution SID is retrieved using CZI images. The SID products based on radiometer or scatterometer are incomparable with the retrieved SID due to the spatial resolution differences. Therefore, the SAR-based SID product (10 km) published by CMEMS is selected for comparison. The reliability of the CMEMS product has been verified in the released user manual (European Union-Copernicus Marine Service, 2015).

- Deleted: N
- Deleted: ing
- Deleted: ing
- Deleted: ing
- Deleted: the method
- Deleted: comprehensive
- Deleted: Jointing
- Deleted: s
- Deleted: s
- Deleted: their
- Deleted: parametric
- Deleted: ing
- Deleted: ing enhances the quality of the results, but it also
- Deleted: blank
- Deleted: appearing in
- Deleted: neighboring
- Deleted: ving sea ice drift.
- Deleted: Consequently, robust SID fields are generated.
- Deleted: the
- Deleted: with a resolution of approximately 4 km
- Deleted: dataset
- Deleted: se
- Deleted: results
- Deleted: image
- Deleted: to
- Deleted: s
- Deleted: , respectively
- Deleted: In this study, h
- Deleted: fields are
- Deleted: with a resolution of approximately 4 km
- Deleted: se
- Deleted: data cannot be compared to SID in this study
- Deleted: sea ice drift

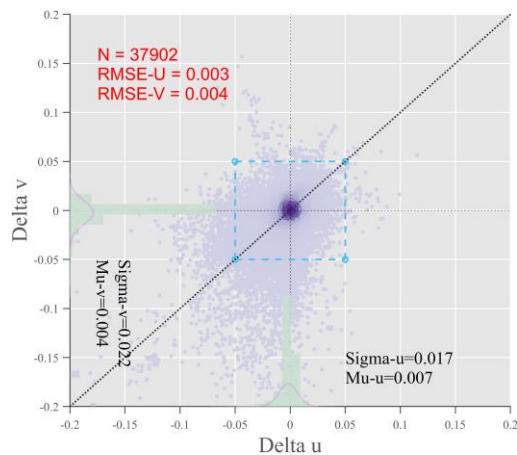
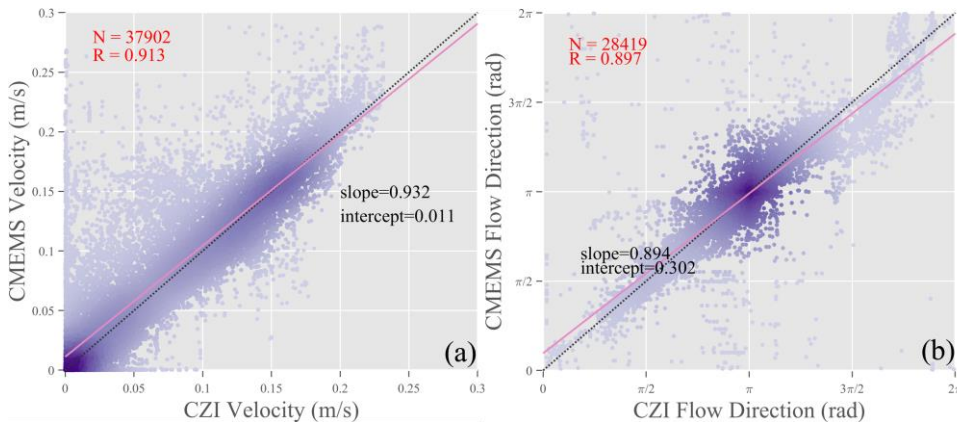


Figure 7: The U-V difference between the retrieved SID (day-level) and the product. The histograms on the x and y axes show the distribution of differences in the U and V directions, and the pink curves fit the histograms. The dashed blue box is 0.05 m/s, and the color shading reflects the density of the scatter distribution.

Fig. 7 shows the U-V difference between the retrieved SID (day-level) and the CMEMS SID products, totaling 37,902 matched points. The U-V differences between the retrieved SID and the product are relatively slight. The majority of the U-V differences are less than 0.05 m/s and the majority of the scatter points are distributed in the center of the plot. The RMSE of U and V are 0.003 m/s and 0.004 m/s, respectively. A strong correlation between the product and the retrieved SID is shown by the histograms and accompanying fitted curves with a normal distribution on the X and Y axes.



- Deleted: CMEMS SID
- Deleted:
- Deleted: obtained by CZI
- Deleted: s
- Deleted: CMEMS
- Deleted: s
- Deleted: at a time interval of approximately 24 hours (day-level),
- Deleted: with most
- Deleted: being
- Deleted: plot's
- Deleted: s
- Deleted: -
- Deleted: V for the SID and SAR products is
- Deleted: There is a
- Deleted: CMEMS SID
- Deleted: recovered
- Deleted: SID, which

**Figure 8: The difference in velocity (a) and flow direction (b) between the retrieved SID (day-level) and the product. The dashed line denotes the ideal line, and the pink line denotes the fit line.**

Fig. 8(a) shows the velocity difference between the retrieved SID and the CMEMS SID product, involving a total of 37,902 matched points. The retrieved SID demonstrates a strong correlation with the product in terms of velocity, as indicated by a high correlation coefficient of 0.913 and a fitted line that closely aligns with the ideal line. The statistics of the difference between the retrieved SID and the product are presented in Table 2, revealing RMSE of 0.003 m/s for the U component, 0.004 m/s for the V component, and 0.005 m/s for the velocity. These slight differences reflect the consistency between the retrieved SID and the product.

The size of the template and search area is associated with the spatial resolution of result. To retrieve high spatial resolution SID in the FS, limited template size and search area is set in our study. Therefore, the maximum velocity of day-level result is lightly smaller than the product. The effect of template size and search area on retrieving SID will be explored in future research. Fig. 8(b) shows the flow direction difference between the retrieved SID and the product using a total number of 28419 matched points. The correlation of the flow direction between the retrieved SID and the product is great, as indicated by a correlation coefficient of 0.897. The statistics of the difference in flow direction between the retrieved SID and the product are shown in Table 2.

**Table 2: Validation of the retrieved SID (day-level) with the product.**

Delta	Number of match point	BIAS	MAE	STD	RMSE
U (m/s)		-0.003	0.009	0.017	0.003
V (m/s)	37902	-0.004	0.013	0.024	0.004
Velocity (m/s)		-0.005	0.014	0.027	0.005
Flow direction (rad)	28419	0.009	0.147	0.369	0.009

Regarding of flow direction, the flow direction of sea ice motion in the FS predominantly ranges from  $\pi/2$  to  $3\pi/2$  (with the positive y-axis as the starting point in polar stereographic projection). The most abundant flow direction is  $\pi$ , which indicates the southern part of the FS. In the comparison of flow direction, it is observed that the shelf ice on the east coast of Greenland has a slower velocity (less than 500 m/day) than the drift ice in the strait. Due to the potential inaccuracy associated with short sea ice displacement, a shelf ice mask was established to exclude the slow-moving shelf ice. The impact of sea ice displacement on retrieval accuracy is analyzed in the discussion section.

- Deleted: CMEMS SID
- Deleted: identity
- Deleted: The
- Deleted: which includes
- Deleted: , is illustrated in Figure 8(a)
- Deleted: superior
- Deleted: velocity
- Deleted: CMEMS SID
- Deleted: al
- Deleted: information on
- Deleted: CMEMS SID
- Deleted: is
- Deleted: values
- Deleted: overall
- Deleted: respectively
- Deleted: CMEMS SID.
- Deleted: Previous studies have shown that CMEMS products have a maximum velocity of approximately 0.4 m/s in the FS (Qiu and C...
- Deleted: CMEMS SID
- Deleted: CMEMS SID
- Deleted: excellent
- Deleted: with
- Deleted: al information
- Deleted: on
- Deleted: CMEMS
- Deleted: is
- Deleted: , with the RMSE of the flow direction being 0.008 rad
- Deleted: CMEMS SID
- Deleted: the
- Deleted: sea ice
- Deleted: flows
- Deleted:
- Deleted: s
- Deleted: exhibits
- Deleted: velocities
- Deleted: (greater than 5000 m/day)
- Deleted: inaccuracies
- Deleted: s
- Deleted: has
- Deleted: will be

#### 4.1.2 SID with the hours-level time interval

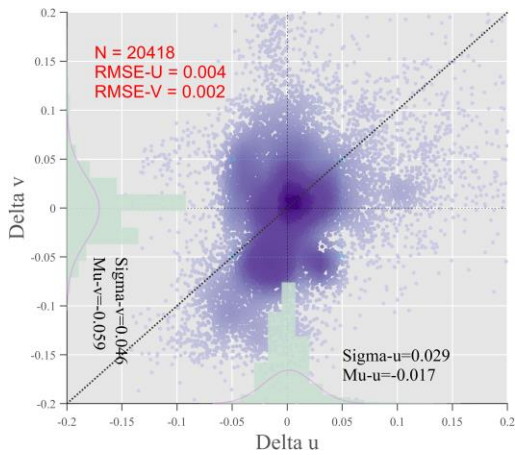


Figure 9: The U-V difference between the retrieved SID (hours-level) and the product. The histograms on the x and y axes show the distribution of differences in the U and V directions, and the pink curves are a fit to the histograms. The dashed blue box is 0.05 m/s, and the color shading reflects the density of the scatter distribution.

Fig. 9 illustrates the difference in U-V between the retrieved SID (hours-level) and the CMEMS SID product, with a totaling 20,418 matched points. The scatter points distribution of the U-V differences in Fig. 9 appears to be significantly more dispersed than that in Fig. 7, suggesting a notable disparity between the retrieved SID and the product. The apparent difference may be associated with the spatial and temporal variability of sea ice motion and will be explicitly analyzed in the discussion section.

- Deleted: CMEMS SID
- Deleted:
- Deleted: shows
- Deleted: for time intervals of less than 6 hours (hours-level),
- Deleted: (
- Deleted: 8)
- Deleted: that
- Deleted: (7)
- Deleted: disparities
- Deleted: at the hours-level
- Deleted: CMEMS SID
- Deleted: s
- Deleted: variabilities
- Deleted: in

## 4.2 Comparison of results with IABP buoys

### 4.2.1 SID with the day-level time interval

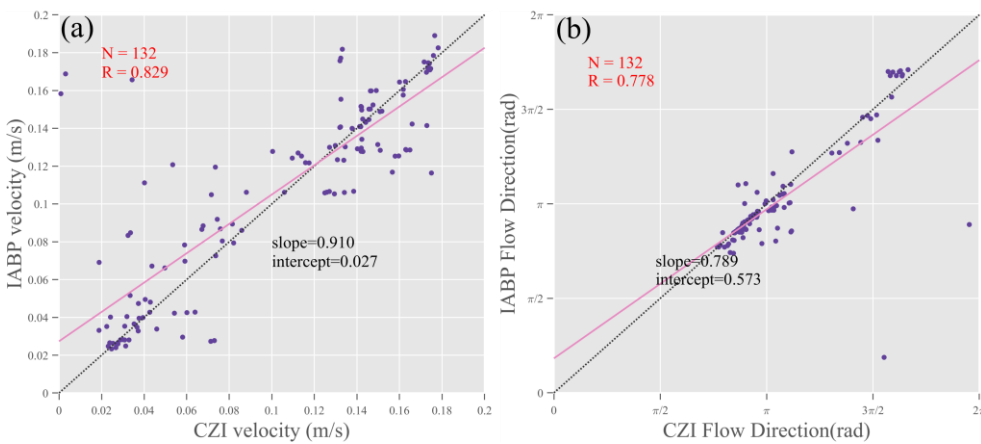


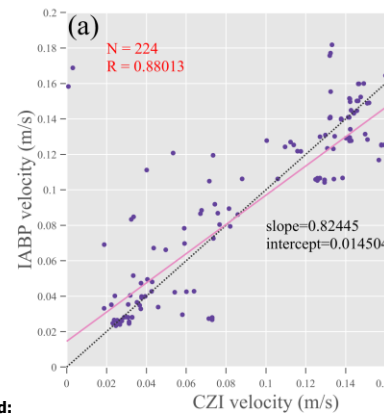
Figure 10: Comparisons between the retrieved SID (day-level) and IABP buoys in velocity (a) and flow direction (b); the dashed line denotes the ideal line, and the pink line denotes the fit line.

The GPS position of the buoys serves as a crucial reference for validating the accuracy of the retrieved SID. Fig. 10 illustrates the difference in velocity (a) and flow direction (b) between the result (day-level) and buoys, with a total of 132 matched points.

The correlation coefficient between the retrieved SID and the buoy of velocity is approximately 0.829, while it is approximately 0.778 for the flow direction. With the time interval of images being approximately 24 hours (day-level), there is a strong correlation between the retrieved SID and the buoy.

Table 3 shows the statistics of the retrieved SID and the buoy, which indicate that the bias is approximately -0.005 m/s and the RMSE is approximately 0.031 m/s for velocity; moreover, for the flow direction, the bias is 0.002 rad and the RMSE is 0.009 rad.

Deleted: s



Deleted:

Deleted: the ...elocity magnitude ...a) and flow direction (b); the dashed line denotes the identity

Deleted: ing information...of the buoys serves as a crucial reference for validating the accuracy of the retrieved SID. Fig. 10 illustrates the difference in velocity (a) and flow direction (b) between the results...of the...day-level) and buoys measurements... with a total of 224...32 matched points. The correlation coefficient between the retrieved SID and the buoy vector for ...f velocity is approximately 0.880...29, while it is approximately 0.924...78 for the flow direction. With the time interval of images being approximately 24 hours (day-level), there is a strong correlation between the retrieved SID and the buoy vector...

Deleted: presents ...hows the statistics...of the retrieved SID at the day-level... and the buoy measurements... which indicating ...ndicate that a ...he bias value of ...s approximately -0.004...05 m/s and an ...he RMSE value of ...s approximately 0.027...31 m/s for velocity;...as well as...oreover, for the flow direction, a ...he bias value of...s approximately ...057...02 rad and an ...he RMSE value of...s approximately ...313...09 rad for flow direction...

**Table 3: Validation of the retrieved SID (day-level) with IABP buoys.**

Delta	Number of match point	BIAS (Relative deviation <sub>mean</sub> )	MAE	STD	RMSE
Velocity (m/s)		-0.005(-1.330%)	0.018	0.031	0.031
Flow direction (rad)	132	0.002(0.149%)	0.003	0.009	0.009

#### 4.2.2 SID with the hours-level time interval

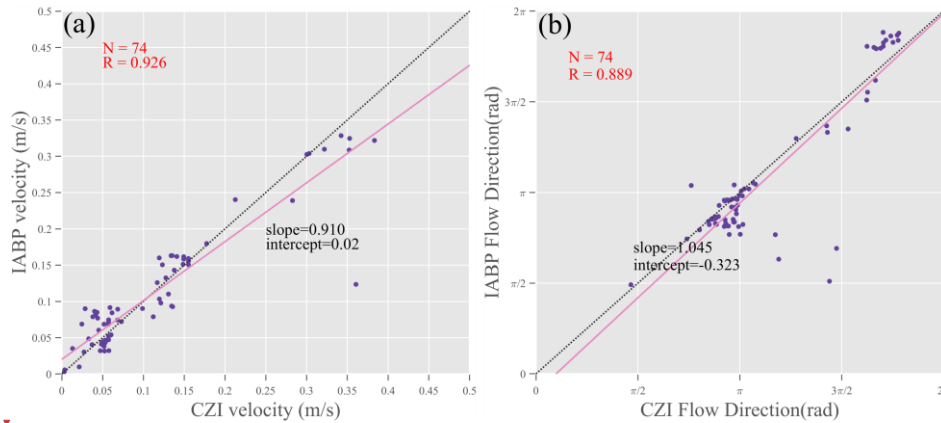


**Figure 11: Comparisons between the retrieved SID (hours-level) and IABP buoys in velocity (a) and flow direction (b); the dashed line denotes the ideal line, and the pink line denotes the fit line.**

Fig. 11 shows the difference in velocity (a) and flow direction (b) between the result (hours-level) and buoys, with a total of 74 matched points. The correlation coefficient of the velocity between the retrieved SID and the buoy is 0.926, and the correlation coefficient of the flow direction between the retrieved SID and the buoy is 0.889. When the time interval of the images is less than 6 hours (hours-level), there is a satisfactory correlation between the retrieved SID and the buoy.

Table 4 provides the statistics of the retrieved SID and the buoy, revealing negligible bias values (~0 m/s) along with a RMSE of 0.036 m/s for velocity. The bias is 0.003 rad and the RMSE is 0.010 rad for flow direction. [Wang et al.] evaluated six SID products over the East Greenland with buoys and found that the MAEs of velocity for these products are ranged from 0.016-0.120 m/s and the MAEs of flow direction are ranged from 0.300-0.973 rad (Wang et al., 2022). Combined with Table 3 and

Formatted: Font: (Default) Times New Roman, (Asian) Times New Roman

Deleted: 004

Deleted: 017

Deleted: 026

Deleted: 027

Formatted: Font: (Default) Times New Roman, (Asian) Times New Roman

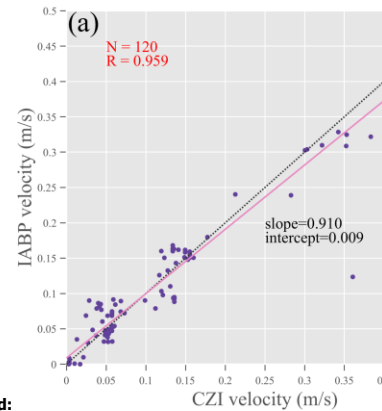
Deleted: 224

Deleted: 057

Deleted: 143

Deleted: 308

Deleted: 313



Deleted:

Deleted: the ...elocity magnitude ...a) and flow direction (b); the dashed line denotes the identity

Deleted: s...of the ...hours-level) and buoys measurements... with a total of 120 ...4 matched points. The correlation coefficient of the velocity between the retrieved SID and the buoy vector ...s 0.924...26, and the correlation coefficient of the flow direction between the retrieved SID and the buoy is 0.897...89. When the time interval of the images is less than 6 hours (hours-level), there is a satisfactory correlation between the retrieved SID and the buoys' vector...

Deleted: s...of the retrieved SID at the hours-level ...nd the buoy vector... revealing negligible bias values (~0 m/s) along with an ... RMSE value ...f 0.022 ...36 m/s for velocity; similarity...there exists the...he bias value of...s 0.011 ...03 rad and the ...he RMSE isof...0.613 ...10 rad for flow direction. [Wang et al.] evaluated eleven ...ix satellite ...ID products over the East Greenland with buoys data ...nd found that the MAEs of velocity for these products are ranged from 0.016-0.120 m/s and the MAEs of flow direction (...)

Table 4, it can be seen that the velocity and flow direction MAEs of our result are smaller than SID products based on radiometer, scatterometer and AVHRR.

Table 4: Validation of the retrieved SID (hours-level) with IABP buoys.

Delta	Number of match point	BIAS (Relative deviation <sub>mean</sub> )	MAE	STD	RMSE
Velocity (m/s)		0.000(1.998%)	0.021	0.036	0.036
Flow direction (rad)	74	0.003(0.154%)	0.006	0.010	0.010

## 5 Discussion

### 5.1 Analysis of the differences between the retrieved SID and the CMEMS SID product

#### 5.1.1 Comparison of individual retrieved SID and the product

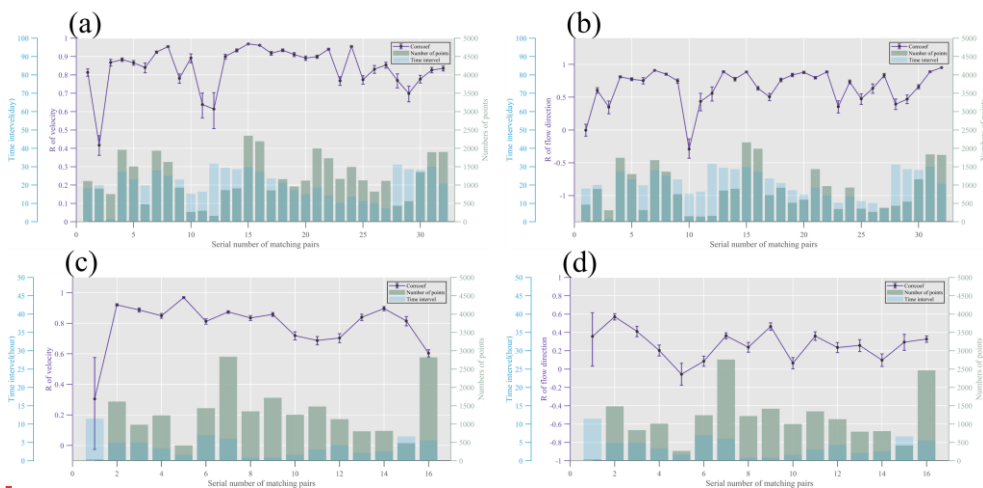


Figure 12: The correlation coefficient and 95% confidence level bar of correlation coefficient between the retrieved SID and the CMEMS SID product. (a), (b): The correlation coefficient between the retrieved SID (day-level) and the product in terms of velocity

Deleted: 5

Deleted: s

Deleted: significantly

Deleted: those of

Deleted: s and

Deleted: s

Deleted: 017

Deleted: 022

Deleted: 022

Deleted: 120

Deleted: 011

Deleted: 371

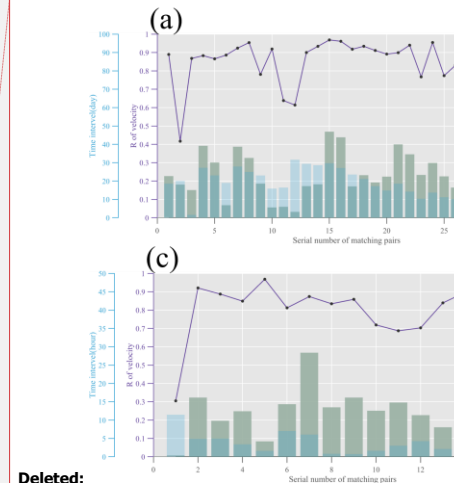
Deleted: 634

Deleted: 631

Deleted: s

Deleted: each

Deleted: CMEMS SID



Deleted:

Deleted: ,

Deleted: the

Deleted: CMEMS SID

and flow direction. (c), (d): ~~The correlation coefficient between retrieved SID (hours-level) and the product in terms of velocity and flow direction. The green histogram (right axis) shows the number of matched points between the retrieved SID and the product, and the blue histogram (the first left axis) shows the time interval between the retrieved SID and the product.~~

The statistics of the retrieved SID and the CMEMS SID product are analyzed in section 4. In this section, we compare the retrieved SID with the corresponding product in chronological order. Fig. 12(a) shows the velocity correlation coefficient curve between the day-level results and the product. Most of the correlation coefficients are greater than 0.7, the bars of 95% confidence level are idealistic. When the correlation coefficient is high, the bar of 95% confidence level is also behave relatively small. However, the 11<sup>th</sup> and 12<sup>th</sup> data pairs exhibited significantly lower correlation coefficients, primarily due to the involvement of fewer matched points (less than 500). Additionally, the correlation coefficient of the 2<sup>nd</sup> data pair is much lower than that of other data pairs due to the dense cloud in the CZI images, which affects the retrieval of SID. Fig. 12(b) shows the correlation coefficient curve of the flow direction between the day-level results and the product. The correlation coefficient of the 10<sup>th</sup> pair is negative and considerably different from that of other data because there are fewer matched points (less than 500). Furthermore, the retrieved SID of 10<sup>th</sup> is located on the northeast coast of Greenland. As the region where TPD encounters the Greenland coastline, the sea ice motion in the region is mutable. The sea ice motion trend in the area is highly variable due to the influence of wind and other forces. The finding reveals that interactions between sea ice in the northern FS, where MYI congregates, can drastically affect the flow direction of the SID. Fig. 12(c) shows the velocity correlation coefficient curve between the hours-level results and the product. The significantly lower correlation coefficient of the 1<sup>st</sup> pair of data can be attributed to the fact that there are not enough matched points (less than 200), and the confidence level bar of the 1<sup>st</sup> pair is also unsatisfactory. Fig. 12(d) shows the correlation coefficient curve of the flow direction between the results (hours-level) and the product. The correlation between the retrieved SID (hours-level) and the product in the flow direction is worse by comparing (b) and (d).

**Deleted:** the ...he correlation coefficient between retrieved SID (hours-level) and CMEMS SID...he product in terms of velocity and flow direction. The green histogram (right axis) shows the number of retrieved SID and CMEMS SID ...atched points between the retrieved SID and the product, and the blue histogram (the first left axis) shows the time interval between the retrieved SID and CMEMS SID input images

**Deleted:** s...of the retrieved SID results ...nd the CMEMS SID product are analyzed in section 4. In t...is section, we compares...the retrieved SID results...with the corresponding CMEMS SID ...roduct in chronological order. Fig. 12(a) shows the velocity correlation coefficient curve between the day-level results and the CMEMS SID ...roduct. Most of the correlation coefficients are greater than 0.7, the bars of 95% confidence level are idealistic. When the correlation coefficient is high, the bar of 95% confidence level is also behave relatively small...However, the 11<sup>th</sup> and 12<sup>th</sup> data pairs exhibited significantly lower correlation coefficients, primarily due to the involvement of fewer matched points (less than 500). Additionally, The 11<sup>th</sup> and 12<sup>th</sup> data pairs, on the other hand, have correlation coefficients that are much lower because there are significantly fewer matched points (less than 500) involved. ...T...e correlation coefficient of the 2<sup>nd</sup> data pair is much lower than that of the...that of other data pairs due to the dense clouds...in the CZI images, which affects the final ...etrieval results...f SID. Fig. 12(b) shows the correlation coefficient curve of the flow direction between the day-level results and the CMEMS SID ...roduct. The correlation coefficient of the 10<sup>th</sup> pair is negative and considerably different from that of the ...ther datas...due ...ecauseto the fact that...there are less ...ever matched points...in this pair ...less than 500). Additionally...urthermore, the retrieved SID of 10<sup>th</sup> is located on the northeast coast of Greenland. As T...e region is ...here the ...PD and ...ncounters the Greenland's coast meet...coastline, and ...he sea ice movements ...otion in the region is unpredictable...utable. The sS...a ice movement ...otion trend in the area is highly variable ...ariaible due to the influence of winds...and other forcing...orces. This ...he finding reveals that interactions between sea ice in the northern FS, where MYI congregates, can drastically affect the flow direction of the SID. According to the CMEMS SID product and our results, sea ice interactions cause the flow direction of SID in the northern half of the FS to be more irregular than in the center part of the Strait...Fig. 12(c) shows the velocity correlation coefficient curve between the hours-level results and the CMEMS SID ...roduct. The significantly lower correlation coefficient of the 1<sup>st</sup> pair of data can be attributed to the fact that there are n't

**Formatted:** Superscript

**Deleted:** at ...the ...ours-level) and the CMEMS SID ...roduct. The correlation between the result at the hours-level...etrieved SID)...(hours-level) and the CMEMS SID

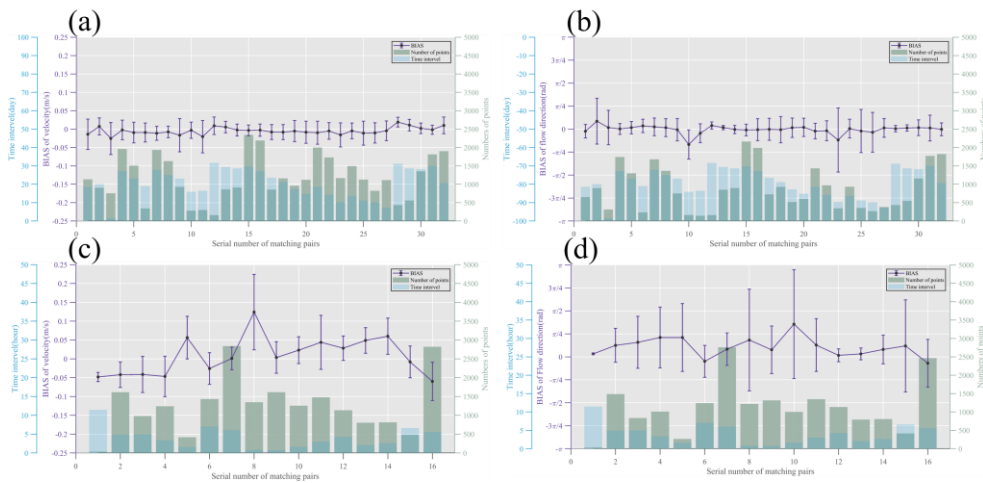


Figure 13: The bias and standard deviation between the retrieved SID and the CMEMS SID product, (a), (b): The bias between the retrieved SID (day-level) and the product in terms of velocity and flow direction. (c), (d): The bias between retrieved SID (hours-level) and the product in terms of velocity and flow direction. The green histogram (right axis) shows the number of retrieved SID and the product matched points, and the blue histogram (the first left axis) shows the time interval between the retrieved SID and the product.

The bias and standard deviation of the velocity between the day-level results and the CMEMS SID product are shown in Fig. 13(a). The velocity bias of the two SID datasets is less than  $\pm 0.05$  m/s, demonstrating a high degree of consistency. When the time interval is large (12<sup>th</sup> and 28<sup>th</sup> pairs) or there are fewer matched points (3<sup>rd</sup>, 10<sup>th</sup>, 11<sup>th</sup> and 13<sup>th</sup> pairs), the bias and standard deviation between our results and the products increase. Fig. 13(b) shows the bias and standard deviation of the flow direction between the day-level results and the product. The bias of the flow direction is slight. When there are fewer matched points (3<sup>rd</sup>, 10<sup>th</sup> and 23<sup>rd</sup> pairs), the bias and standard deviation of the flow direction become larger. Fig. 13(c) shows the velocity bias and standard deviation between the hours-level results and the product. Although most of the bias are smaller than 0.15 m/s, the velocity bias is significantly more substantial than that of the day-level result. The bias and standard deviation of the flow direction between the results (hours-level) and the product are shown in Fig. 13(d). By comparing (a), (b) and (c), (d) in Fig. 13, the day-level results are much less divergent from the product than the hours-level results.

### 5.1.2 Analysis of the difference

The day-level results are compared to the CMEMS SID product in Fig. 7 and 8, revealing the slight difference in U, V, velocity, and flow direction. The statistics in Table (2), also illustrate the slight difference between our results and the product. However, Fig. 12 shows a significant difference between the hours-level result and the product. The retrieval methods used in our study

- Deleted: the
- Deleted: CMEMS SID
- Deleted: the
- Deleted: CMEMS SID
- Deleted: CMEMS SID
- Deleted: CMEMS SID input images
- Deleted: difference
- Deleted: data
- Deleted: deviation
- Deleted: of
- Deleted: CMEMS SID
- Deleted: become greater
- Deleted: deviation
- Deleted: CMEMS SID
- Deleted: deviation
- Deleted: in
- Deleted: However, w
- Deleted: deviation
- Deleted: deviation
- Deleted: CMEMS SID
- Deleted: es
- Deleted: data
- Deleted: variation
- Deleted: at the
- Deleted: CMEMS SID
- Deleted: CMEMS SID
- Deleted: are presented
- Deleted: s
- Deleted: between them
- Deleted: Table (2) statistics
- Deleted: minute
- Deleted: s
- Deleted: CMEMS SID
- Deleted: s
- Deleted: s
- Deleted: CMEMS

differed slightly from the method of the product, but both algorithms are based on the MCC. This discrepancy may be attributed to either the time interval of SAR images used in the product or the time interval between the two kinds of SID.

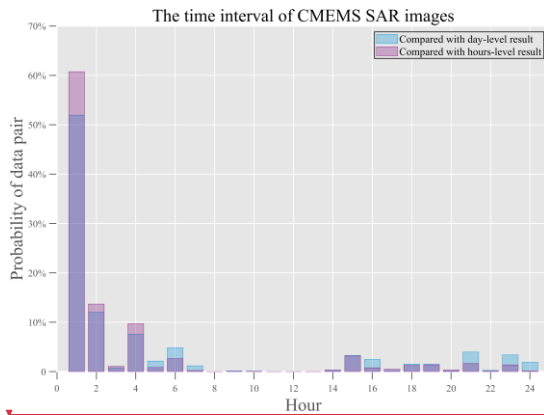
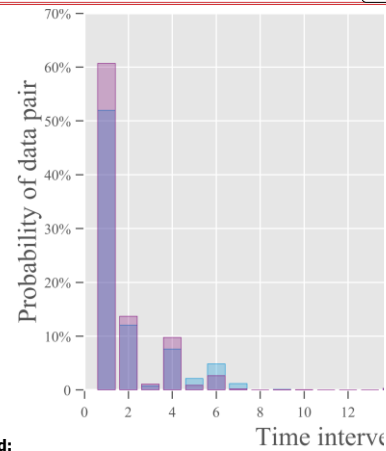


Figure 14: The time interval of SAR images used by the CEMES SID product during the comparison with two different results.

Fig. 14 shows the time interval of SAR images used by the CEMES SID product. The blue histogram represents the time interval of the SAR images used by the product, which is compared to the day-level result, and the purple histogram represents the time interval of the SAR images used by the product, which is compared to the hours-level result. Fig. 14 shows that the blue and purple histogram distributions are nearly identical. Most time intervals of SAR image used by the product are less than 6 hours, and only a few are approximately 20 hours. The consistent distribution trend of the two kinds of histograms indicates that the time intervals of the SAR images used by the product are basically the same. The distribution of the histograms explains that the difference between the retrieved SID and the product is not relevant to the time interval of the SAR images used by the product.

**Deleted:** those of...the method of CEMES SID...he products... but both algorithms are based on the the ...CC. These...discrepancy may be attributed to either the time interval of SAR images used in the CEMES SID ...product or the time interval between the images used by the ...etween the two kinds of SID results



**Deleted:** for ...y the CEMES SID products... The blue histogram represents the time interval of the SAR images of ...sed by the CEMES SID ...product, which is used for the...ompared comparison with ...o the day-level results... and the purple histogram represents the time interval of the SAR images of ...sed by the CEMES SID ...product, which is used for the comparison...ompared with ...o the hours-level results... Fig. 14 shows that the blue and purple histogram distributions are nearly identical. Most time intervals of SAR image time intervals ...sed in ...y CEMES SID...he products...are less than 6 hours, and only a few are approximately 20 hours. The consistent distribution trend of the two kinds of histograms indicates that the time intervals of the SAR images used by the CEMES SID ...roducts

**Deleted:** two...histograms explains that the difference between the retrieved SIDresults...and the CEMES SID ...roducts

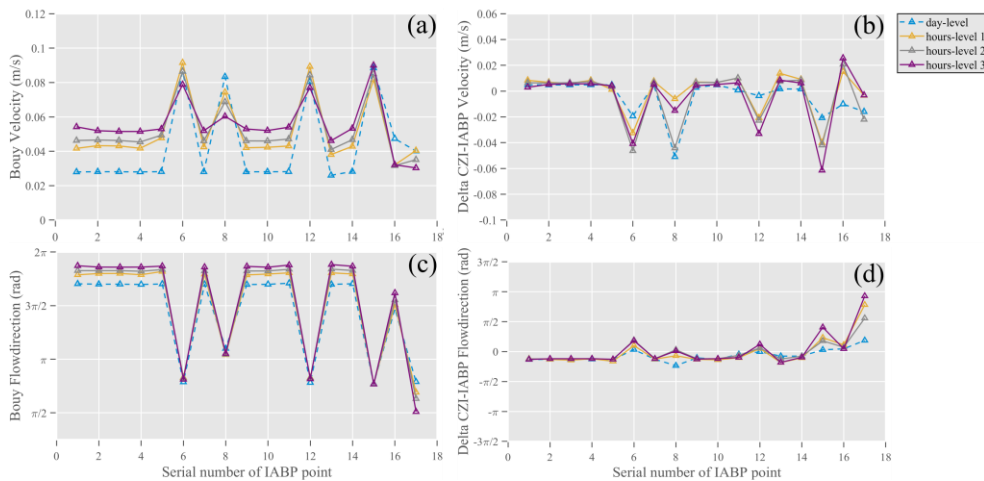


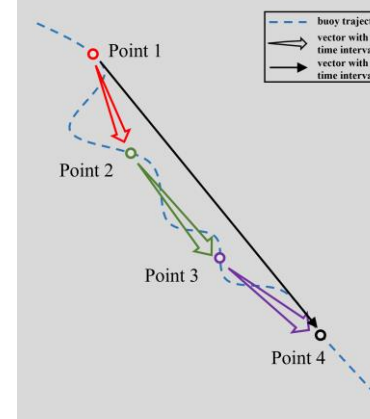
**Figure 15:** The buoy velocity (a) and flow direction (c) and the difference (velocity (b), flow direction (d)) between the retrieved SID and buoys. The lines in blue represents SID and buoy vectors with day-level time interval and the lines in yellow, gray and purple represents SID and buoy vectors with hours-level time interval on the same day. The x-axis shows the different matched SID and buoys. The y-axis in (b) and (d) show the difference between SID and buoys.

We attribute the difference between the hours-level result and the CMEMS SID product to the temporal and spatial variability of sea ice motion. Fig. 15(a) and (c) show the variations in the velocity and flow direction of 17 different buoys with different time intervals. The date of day-level CZI images are 06 April 2021, 06:10:12 LT and 07 April 2021, 07:16:35 LT. The first date of the hours-level CZI images are 06 April 2021, 06:10:12 LT and 06 April 2021, 09:29:35 LT, the second date of the hours-level CZI images are 06 April 2021, 06:10:12 LT and 06 April 2021, 11:10:03 LT, and the third date of the hours-level CZI images are 06 April 2021, 09:29:35 LT and 06 April 2021, 11:10:03 LT. The triangles in Fig. 15(a) represent the velocity of the buoys, and there is a significant difference in velocity between the day-level buoys and the hours-level buoys. The difference of velocity between hours-level buoys is less than the difference between hours-level buoys and day-level buoys, but the difference still exists. The same trend is also found in the difference of flow direction as shown in Fig. 15(c). Fig. 15(b) and (d) show the differences in velocity and flow direction between our results and the buoys, and the day-level result deviates less from the buoy. Additionally, different buoys show various differences from our results, which is related to the location of the buoys.

The velocity and flow direction differences of the buoys with different time intervals suggests that SID has large spatial and temporal variability. There is a distinct variability in velocity and flow direction when the SID is retrieved using images with short time interval. When the drift vectors retrieved with longer time interval are compared with those vectors retrieved at shorter intervals, differences are noted. This phenomenon is a consequence of the spatial and temporal variability of SID. When

**Deleted:** The buoy velocity (a) and flow direction (c) and the difference (velocity (b), flow direction (d)) between the retrieved SID and buoys.

**Deleted:** s... and the CMEMS SID product to the temporal and spatial variabilities ... variability in ... of sea ice motion. Fig. 15(a) and (c) show the variations in the velocity and flow direction of 17 different buoys at ... with different time intervals. The date of day-level CZI pair ... images date is ... 06 April 2021, 06:10:12 LT and 07 April 2021, 07:16:35 LT. The first date of the hours-level CZI pair date ... images is ... 06 April 2021, 06:10:12 LT and 06 April 2021, 09:29:35 LT, the second date of the hours-level CZI pair ... images date is ... 06 April 2021, 06:10:12 LT and 06 April 2021, 11:10:03 LT, and the third date of the hours-level CZI pair ... images date is ... 06 April 2021, 09:29:35 LT and 06 April 2021, 11:10:03 LT. The triangles in Fig. 15(a) represent the velocity of the buoys, and there is a significant difference in velocity between the day-level buoys and the hours-level buoys. The difference of velocity between hours-level buoys is less than the difference between hours-level buoys and day-level buoys, but the difference still exists. The same trend is also found in the difference of flow direction as shown in Fig. 15(c). Fig. 15(b) and (d) show the differences in velocity and flow direction between our results and the buoys ... and the day-level result had ... deviates less from smaller difference with ... the buoys ... Additionally, different buoys showed ... various differences from our results ... which are ... related to the location where ... if the buoys are deployed



**Deleted:**

**Deleted:** spatial and temporal variabilities ... velocity and flow direction differences in ... of the buoys and the comparison with our results ... with different time intervals suggest ... suggests that SID has large spatial and temporal variability. As shown by the colorful arrows in Fig. 16, there is a distinct large ... variability in velocity and flow direction when the SID is retrieved using images with short time intervals ... When the drift vectors ... retrieved at ... with longer time intervals ... are compared with those vectors retrieved at shorter intervals, some ... differences are noted. This result ... phenomenon is a consequence of the spatial and temporal variability in

comparing the drift vectors retrieved with two different short time intervals, in extreme situations, a greater difference will be presented. The variability of sea ice motion is more complex and unpredictable on a small time scales. The complex spatial and temporal variability of SID explained the discrepancy between our results and the CMEMS SID product.

Despite the spatial and temporal variability of sea ice motion, it is still important to validate our retrieved results using the product. Furthermore, as long as a sufficiently large time interval is employed, the impact of SID variability diminishes, which results in consistent drift trend being observed. Utilizing SID products for evaluating the retrieved result remains valid while providing valuable references through consistency and difference ratings.

## 5.2 Effect of different time intervals on retrieving SID

In section 5.1, the consistency and discrepancy between the result and the CMEMS SID product is discussed, revealing the spatial and temporal variability of sea ice motion. In this section, we explore the impact of different time intervals on retrieving SID by analyzing the validation of the buoys and the statistics of the quality control parameters. The time interval of CZI images is a factor that affects the accuracy of retrieving SID. On the one hand, elaborate sea ice motion can be tracked by using images with short time interval; on the other hand, retrieving SID from images with longer time interval provides more stable result. Therefore, it is crucial to discuss the appropriate time interval for retrieving SID in FS.

Section 3.3 describes the three parameters used for quality control: R, PMR and PSR. Table 5 presents the statistics of these parameters with different time intervals. Each quality control parameter's mean value of the hours-level result is greater than that of the day-level result, which indicates that the hours-level result has the higher quality. However, the standard deviation of the quality control parameters exhibit opposite trend. The standard deviation of the quality control parameters for the day-level result is smaller than for the hours-level result. The statistics indicate that the day-level result remain relatively stable despite having slightly poorer quality.

Table 5: Statistics of quality control parameters at different time intervals.

Parameter	MEAN	STD	Type
R	0.372	0.199	day-level
	0.473	0.225	hours-level
PMR	9.338	4.857	day-level
	13.262	6.198	hours-level
PSR	1.620	0.838	day-level
	2.016	0.980	hours-level

In the validation with the buoy, the correlation of the day-level result is slightly lower than that of the hours-level result in velocity. In terms of flow direction, the correlation of the day-level result is also lower than that of the hours-level result. The retrieval of day-level SID confronts with the effects of large drift distances, wind change, light variation, cloud, etc., which are disadvantageous for retrieving. The statistics in Tables 3 and 4 also show that the hours-level result possesses better accuracy

**Deleted:** some ...xtreme situations, a large ...reater difference will be presented. due to the spatial and temporal variability in sea ice. ...he variability in ...f sea ice motion SID ...s more complex and unpredictable on a small time scales. The complex spatial and temporal variability in ...f SID explained the discrepancy between the ...ur results of this study

**Deleted:** in ...sea ice motion, it is still importantpossible...to validate our retrieved results using the CMEMS SID ...roduct which remains comparable for this purpose... Furthermore, as long as a sufficiently large time interval is employed, the impact of SID variability diminishes, whiches...resulting ...results in consistent drift trends...being observed. Utilizing SID products for evaluating the retrieved results...remains valid while providing valuable references through consistency ratings...and difference ratings obtained during such comparisons

**Deleted:** The e

**Deleted:** S...ction 5.1 discusses... the consistency and discrepancy between the results...of this study ...nd the CMEMS SID product is discussed, while ...eavealing the spatial and temporal variability in SID...f sea ice motion. In this section, we explore the impact of different time intervals on retrieving SID by analyzing the validation results from...f the buoys and the statisticc...of the quality control parameters. The time interval of CZI images is a critical ...actor in ...hat affects the accuracy of retrieving SID. On the one hand, the process of detailed...laborate sea ice motion SID could...an be by using images with short time intervals... on the other hand, retrieving SID retrieval...from images with longer time interval images ...rovides more stable results... Therefore, it is crucial to determine ...iscuss an ...he appropriate time interval for retrieving SID in the

**Deleted:** s...of these parameters at ...ith different time intervals over the regions that retained valid SID vectors after quality control and neighborhood filtering... As seen from the mean values, e...ach quality control parameter's mean value for ...f the hours-level results...is more significant...reater than for ...hat of the day-level results... which indicates that the hours-level results...possess ...as higher quality. However, the standard deviation of the quality control parameters is...xhibit the...opposite trend. The standard deviation of the quality control parameters for the day-level results...is smaller than for that for ...he hours-level results... The statisticc...indicate that the day-level results

**Deleted:** comparison ...alidation with the buoys... the correlation of the day-level results at the day-level...is slightly lower than that of that at ...he hours-level result in terms of...velocity. In terms of flow direction, the correlation of the day-level results...is also lowerslightly higher... than that of that of ...he hours-level results... The retrieval of images at the ...ay-level is ...ID first ...onfronted... with the effects of large drift distances, wind change, sea ice melt, sea ice break-up... light variations... clouds... etc., which are disadvantageous for retrieving. Therefore, the velocity accuracy of the day-level results is lower than that of the hours-level results....

than the day-level result. Images with short time interval provide a more stable scenes for retrieving SID, thus the hours-level result possesses fine accuracy.

In our study, the dataset was divided into two groups according to the image time interval. In comparison with the buoy, both results achieved great accuracy. According to the analysis of the day-level result and the hours-level result, we believe that retrieving SID using images with short time interval will provide SID with better accuracy. Our propositional time interval is shorter than the time interval proposed by Qiu, who suggested using images with 20-hours time interval to retrieve SID in FS from January to June (Qiu and Li, 2022). We attribute these divergent conclusions on suitable time interval due to the limitations of our dataset. In future studies, we are planning to incorporate HY1-C data and investigate the impact of varying time intervals on SID retrieval.

### 5.3 The potential of retrieving sea ice drift from image with cloud

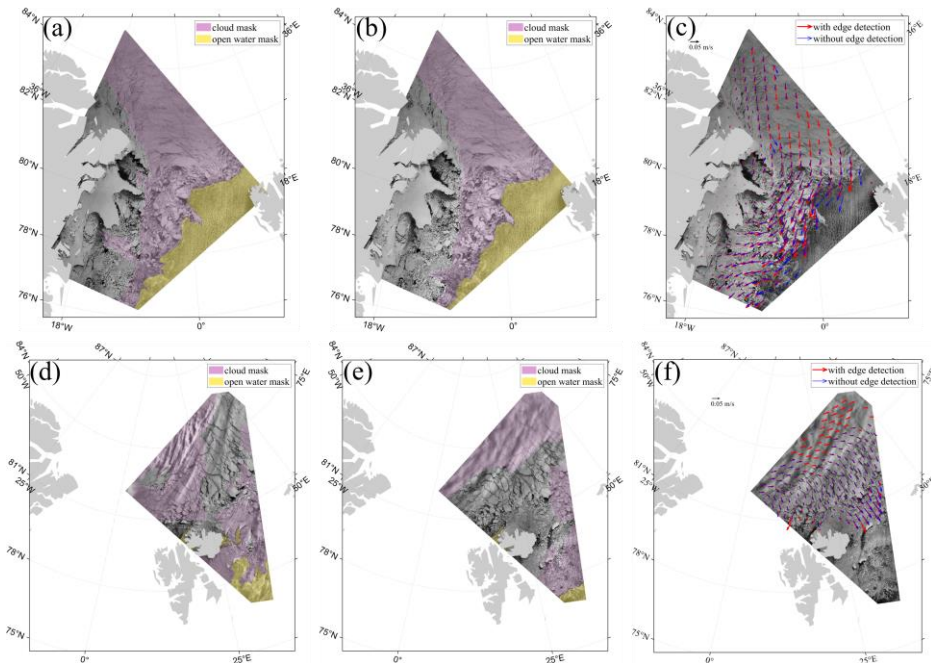


Figure 16: Two examples of retrieving sea ice drift from image with cloud. Images (a), (b), and (c) are a pair of results, and images (d), (e), and (f) are another pair of results. The arrows in (c) and (f) are diluted for direct viewing.

**Deleted:** In the flow direction retrieval, the accuracy of the day-level results is better than that of the hours-level results, which might be relevant in the method of MCC to retrieve the flow direction. When the MCC algorithm retrieves vectors with shorter displacements, a smaller deviation can lead to a larger bias in the flow direction. ...

**Deleted:** (Lavergne et al., 2010)The trends are also supported by statistical parameters in Tables 3 and 4.

**Deleted:** is

**Deleted:** s

**Deleted:** the results of

**Deleted:** datasets

**Deleted:** excellent

**Deleted:** After comparison, we believe that using image pairs with shorter time intervals yields results with high quality but with the disadvantage that the stability of the SID will be poor.

**Deleted:** accuracy

**Deleted:** dataset

**Deleted:** also

**Deleted:** pairs

**Deleted:** greater

**Deleted:** s (greater than 6 hours)

**Deleted:** results

**Deleted:** Our suggestion on time intervals is shorter than the thesis of Qiu, Qiu suggest uses SAR images with about 20 hours to retrieve SID in the FS from January to June (Qiu and Li, 2022).

**Deleted:** s

**Deleted:** the

**Deleted:** limited

**Deleted:** size of our

**Deleted:** the

**Deleted:** studies

**Deleted:** , thereby enhancing the comprehensiveness of our research...

**Deleted:** Adaptability of edge detection

**Deleted:** 17

**Deleted:** with clouds in an image

**Deleted:** , and the open water area in the middle of the sea ice is excluded.

Retrieving SID using optical imagery can be affected by factors such as cloud, lighting and other variables. Sobel edge detection is used to enhance the texture of sea ice. We found that SID result is also achieved for sea ice under cloud after using Sobel edge detection. Fig. 16 shows two examples of SID retrieved from images with cloud. The first example uses hours-level time interval images for retrieval, with image (a) taken on 27 April 2021, 09:27:33 LT and image (b) taken on 27 April 2021, 11:07:20 LT. The second example uses day-level time interval images for retrieval, with image (c) taken on 02 May 2021, 03:20:35 LT and image (d) taken on 03 May 2021, 06:07:37 LT. In the second example, images (d) and (e) are also covered by thick cloud in addition to thin cloud, which more severely obscure the sea ice texture. Fig. 16(a) and (b) show the cloud and open water by visual interpretation. Fig. 16(c) shows the SID vectors derived from the images, where the vectors with Sobel edge detection in the preprocessing are in red, and the vectors without Sobel edge detection are in blue. A comparison of these two types of vectors reveals a more consistent trend of SID with a homogeneous velocity distribution achieved by using Sobel edge detection, which demonstrates that edge detection promotes the retrieval algorithm and illustrates the potential for optical imagery to retrieve SID using images with thin cloud. Fig. 16(d), (e) and (f) show another pair of result using CZI images with the day-level time interval. In contrast to the first pair of result, the CZI images (Fig. 16(d), (e)) have more cloud, and the variation in the cloud distribution is quite apparent. Comparing the vectors with two different colors, the red vector is better, even providing result in parts of the area under thick cloud. Thin cloud is distributed in lower right corner of the image, but the algorithm does not give credible result due to the strongly fragmented sea ice. Analytically, edge detection strengthens the ability of algorithm to retrieve SID from images with cloud. In addition, Fig. 16 similarly shows the enhancement of the separating capacity for open water of algorithm by using detection. The red vectors in Fig. 16(c) and (f) are mainly distributed within the sea ice extent.

**Deleted:** Optical images in r...retrieving SID using optical imagery can be affected by factors such as clouds... lighting and other variables. In this study, ...obel edge detection is used to enhance the texture of sea ice. Through ...experimentation, w... find ...ound that better retrieval results ...ID result are ...s also achieved for sea ice under thin ...louds...after using Sobel edge detection. Fig. 17...6 shows two examples of SID retrieved under ...rom images within...cloud conditions... The first example has ...ses hours-time interval images for retrieval, with image (a) taken at ...n 27 April 2021, 09:27:33 LT and image (b) taken at ...n 27 April 2021, 11:07:20 LT. The second example has ...ses day-level time interval images for retrieval, with image (c) taken at ...n 02 May 2021, 03:20:35 LT and image (d) taken at ...n 03 May 2021, 06:07:37 LT. In the second example, images (d) and (e) are also covered by thick clouds...in addition to...n addition to thin clouds

**Deleted:** 17...6(a) and (b) show the clouds...and open water in the image ...y visual interpretation. Fig. 17...6(c) shows the SID vectors derived from this study... images, where the vectors with Sobel edge detection in the preprocessing are in red, and the vectors without Sobel edge detection are in blue. A ... comparison between ...f these two types of vectors reveals a more consistent trend of SID with a homogeneous velocity distribution achieved through the use of

**Deleted:** . This comparison... which demonstrates that edge detection enhances ...romotes the retrieval algorithm and illustrates the potential for optical data ...magery to retrieve SID using images under ...ith thin cloud conditions... Fig. 17...6(d), (e) and (f) show another pair of results...using CZI images with the day-level time intervals... In contrast to the first pair of results... the CZI images 17...6(d), (e)) have many ...ore clouds... and the variation in ...n the cloud distribution of the clouds ...s very ...uite apparent. Comparing the vectors with two different colors, the red vector using edge detection ...s significantly ...etter, even providing results...in parts of the the ...rea under thick cloud area... There is a t...thin cloud is distributed ...istributed in the image's...lower right corner of the image, but the algorithm does not give credible results...due to the strongly fragmentedheavily broken...sea ice, ... and our algorithm still needs to be improved to address this situation. ...analytically, detection strengthens the capability ...bility of algorithm to retrieve SID from images with clouds... In addition, Fig. 17...6 similarly shows the enhancement of the separating capacity of algorithm ...or open water of algorithm after applying Sobel edge...y using detection. The red vectors in Fig. 17...6(c) and (f) are mainly distributed within the sea ice extent. Overall, applying edge detection in preprocessing helped the algorithm to retrieve high-quality SID...

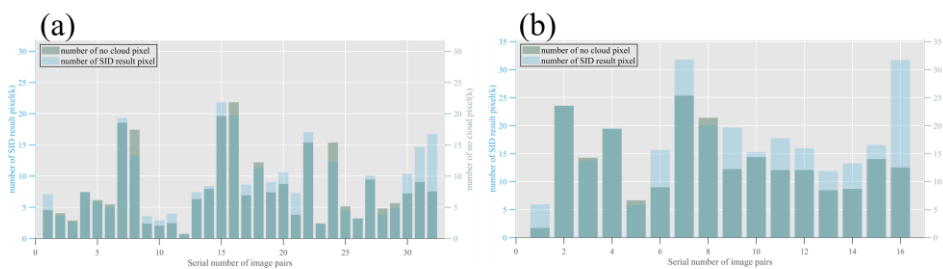


Figure 17: The number of no-cloud pixels (green) and the retrieved SID pixels (blue) (a: day-level result, b: hours-level result).

To quantify the potential of retrieving SID from image with cloud, we use the whiteness index (Gómez-Chova et al., 2008) and Multiscale Edge-preserving Decompositions (MED) (Farbman et al., 2008) to detect the cloud pixels (Kang et al., 2018). Fig. 17(a) and (b) show the number of no-cloud pixels and the number of retrieved SID pixels. For the day-level results, in addition to the influence of cloud pixels, dramatic shape changes of sea ice also hinder the retrieval of SID. As shown in Fig.

17(a), only a few (1<sup>st</sup>, 15<sup>th</sup>, 21<sup>st</sup>, 30<sup>th</sup>, 31<sup>st</sup> and 32<sup>nd</sup>) of the retrieved SID pixels are beyond the no-cloud pixels. For the 32<sup>nd</sup> image pair, the number of SID pixels is 120% greater than the number of no-cloud pixels, possibly because the cloud in the images is quite thin. For the hours-level results, images with short time interval provide a stable scene for retrieving. Thus, many of the retrieved SID pixels (1<sup>st</sup>, 6<sup>th</sup>, 7<sup>th</sup>, 9<sup>th</sup> and 11<sup>th</sup>-16<sup>th</sup>) are greater than the no-cloud pixels as shown in Fig. 17(b). For the 16<sup>th</sup> image pair, the number of retrieved SID pixels is 150% greater than the number of no-cloud pixels, this is because the cloud is slight and the distributions of cloud in two images are similar. The average of SID pixels beyond the no-cloud pixels is 10.109% and 28.920% for the day-level result and the hours-level result, respectively. In conclusion, our approach has the potential to retrieve SID effectively with images containing cloud pixels. The result shows that with less strict restriction and appropriate preprocessing, images with cloud could be used to obtain credible and dense SID.

#### 5.4 Factors affecting the accuracy of flow direction retrieval

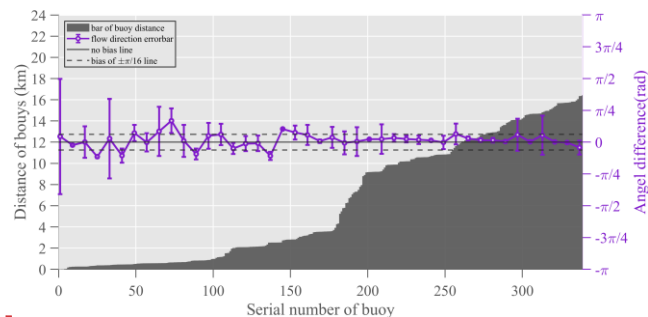
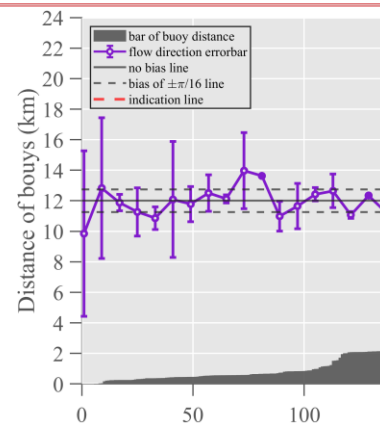


Figure 18: Relationship between the flow direction and the displacement of the buoys.

Qiu concluded that the flow direction accuracy of the retrieved SID is associated with the magnitude of the velocity (Qiu and Li, 2022). In our study, when dividing the dataset into hours-level and day-level by time interval for comparison with the buoys, inconsistent conclusion was found when analyzing the accuracy of flow direction. Compared with the buoy data, the statistics in flow direction of the SID at day-level is slightly smaller than the SID at hours-level. However, since the coverage areas of both datasets are repetitive, the magnitudes of velocity retrieved from both datasets should be the same. Thus, it is not the velocity magnitude of the SID that affects the accuracy of the flow direction retrieval.

We consider that the distance of sea ice motion affects the accuracy of the flow direction retrieval. Due to stochastic error, the identification of the highest correlation point deviates to the optimal point. Consequently, the retrieved flow direction is constrained to the vicinity of the optimal point. The variability of flow direction retrieval with longer distance is more stable than with shorter distance. Retrieving the flow direction precisely with small displacement is challenging, and the time interval needs to be increased to achieve longer sea-ice displacements, although this can also lead to other disadvantages (e.g., cloud disintegration) for SID retrieval. Fig. 18 shows the relationship between the drift distance of the buoys and the difference,

Deleted: (Gómez-Chova et al., 2008)(Farbman et al., 2008)(Kang et al., 2018)(Gómez-Chova et al., 2008)(Farbman et al., 2008)(Kang et al., 2018)



Deleted: Ser

Deleted: The r

Deleted: [...] concluded that the flow direction accuracy of the retrieved SID is associated with the magnitude of the velocity (Qiu and Li, 2022). In our study, when dividing the dataset into hours-level and day-level by time interval for comparison with the buoys, inconsistencies were found when analyzing the accuracy differences. In the flow directions... Qiu's conclusions are also found when analyzing the accuracy differences in the retrieving flow directions... Compared with the buoy data, the statistics difference in the flow direction of the SID at the day-level is slightly smaller than that of the SID at the hours-level. However, since the coverage areas of both datasets are repetitive, the magnitudes of velocity retrieved from both datasets should be the same. Thus, it is not the velocity magnitude of the SID that affects the accuracy of the retrieving

Deleted: Our study considers that the distance of sea ice displacement motion affects the accuracy of the flow direction retrieval. Due to stochastic error, the identification of the highest correlation point deviates to the optimal point. Consequently, the retrieved flow direction is constrained to the vicinity of the optimal point. The variability of flow direction retrieval with longer distance is more stable than with shorter distance. Retrieving the precise flow direction precisely with small displacements is challenging, and the time interval needs to be increased to achieve longer sea-ice displacements, although this can also lead to other disadvantages (e.g., clouds, ice breaks, disintegration) for sea-ice SID retrieval. Fig. 18 shows the relationship between the drift distance of the buoys and the differences

between the retrieved SID and the buoy in the flow direction. We generated a total of 206 matched points and merged every 5 points to calculate the standard deviation. As the buoy displacement increases, the bias and standard deviation of the flow direction decrease, which indicates that the accuracy of the retrieved flow direction is affected by the distance of sea ice motion. A larger displacements result in more precise flow direction retrieval, but also require longer time interval images which will introduces disadvantageous factors for algorithm.

### 5.5 Factors affecting the accuracy of velocity retrieval

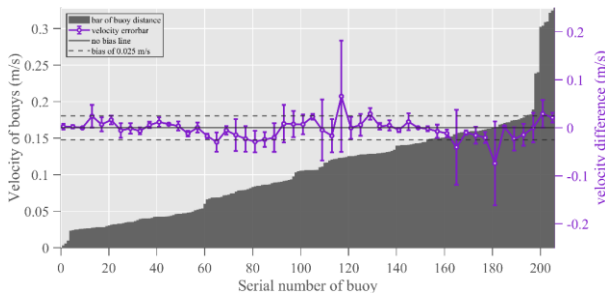


Figure 19: Relationship between the velocity difference and the velocity of the buoys.

The study area spans the Arctic basin to the Fram Strait, where the velocity of the SID generally presents complicated variations. The maximum magnitude of buoy-derived ice velocity can reach to 0.64 m/s in FS (Lei et al., 2016). Sea ice in the north of the FS or close to the land has a relatively low velocity. It is imperative to make further research on the accuracy of retrieving SID with different velocity.

In our study, the data were from March to May 2021, and we generated a total of 206 matched points and merged every 4 points to calculate the standard deviation of the velocity difference. We further analyzed the relation between the accuracy of retrieved velocity and the buoy velocity. As shown in Fig 19, the bar shows that the velocity of buoys that we used in validation ranged from 0 m/s to 0.32 m/s, and the line of bias and standard deviation shows the accuracy of the retrieved velocity which is associated with the velocity of the buoys. As the velocity of the buoys increases to 0.1 m/s, both the bias and standard deviation also increase. Although the bias of retrieved velocity occurs within in an ideal range as the velocity of the buoys increases, the standard deviation of the velocity difference becomes erratic. In general, sea ice motion with great velocity appears unstable in the images. Our algorithm still need improvement in retrieving SID with high velocity.

Deleted: vectors

Deleted: 344

Deleted: are

Deleted: 8

Deleted: bias and

Deleted: the

Deleted: displacement

Deleted: L

Deleted: accurate

Deleted: s

Deleted: s

Deleted: with more

Deleted: performance

Deleted: Therefore, satisfactory accuracy of flow retrieval can be achieved by controlling the time interval to a displacement of greater than 3 km (approximately 10 pixels in the images), as indicated by the red dashed line in Fig. 18.

Formatted: Caption

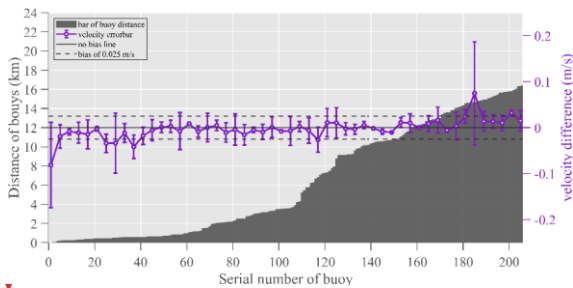


**Figure 20: Relationship between the velocity difference and the displacement of the bouys.**

1180 Additionally, we delve into the correlation between the distance of sea ice motion and the accuracy of the retrieved velocity. A significant challenge to the accuracy of velocity retrieval, as emphasized by Lavergne, is the presence of quantification noise in template matching (Lavergne et al., 2010). Despite the acknowledged presence of quantification noise, our result surprisingly does not reveal its discernible effects, and a lack of a statistically significant correlation between the accuracy of the retrieved velocity and buoy distance is observed (As shown in Fig. 20).

1185 Several explanations underpin this result. First, the spatial resolution of the resampled CZI imagery is 300m, which is a notable improvement for the ice surface feature observation compared to the kilometer-level resolution of radiometer. The higher spatial resolution is posited to be a key factor limiting the manifestation of quantification noise. The topographic features of sea ice are often quantified by the surface roughness and form drag (Arya, 1973, 1975) and those observed surface features have impact on ice drift speed (Zu et al., 2021). The form drag can be decomposed into the contributions from ridges, snow dunes etc., and it is associated with the momentum exchange between sea ice and the lower atmosphere forced by wind (Zhang et al., 2024). The topographic features (including height and spacing) within the optical imagery need to be described quantitatively in the future work. Second, the strong sea ice motion in FS renders sea ice dynamics distinctly visible in the image, indirectly suppressing the appearance of quantification noise. Finally, our application of subpixel estimation for the precise localization of maximum correlation values, results in an exact determination of the maximum correlation location. This refinement contributes to improve the accuracy of retrieving SID. In conclusion, high spatial resolution data and subpixel estimation are able to suppress the negative effects caused by quantification noise.

### 5.6 The parameters for quality control

1200 To validate the effectiveness of quality control parameters, a comprehensive examination was undertaken, involving a comparative analysis between the quality control parameters and buoy validation of the SID. The red line in Fig. 21 shows the R of the validation points, and to identify the relationships between R and the other parameters, the data are sorted in ascending order by R. The bar in orange and bar in blue represent the PMR and PSR, respectively. The figure revealed a pronounced congruence, wherein the R, PMR and PSR exhibited coherent consistency. A positive correlation was discerned, indicating

Deleted: (Lei et al., 2016)

Formatted: Font: (Default) Times New Roman, 10 pt, Font colour: Auto

Formatted: Font: (Default) Times New Roman, 10 pt, Font colour: Auto

Formatted: Font: (Default) Times New Roman, 10 pt, Font colour: Auto

Formatted: Font: (Default) Times New Roman, 10 pt, Font colour: Auto

Formatted: Font: (Default) Times New Roman, 10 pt, Font colour: Auto

Formatted: Font: (Default) Times New Roman, 10 pt, Font colour: Auto

that the increase in R proportionally accompanies the increase in the PMR and PSR. The magnitude of R has been extensively used as a quality control parameter for SID retrieval (Qiu and Li, 2022; Haarpaintner, 2006; Robert Ezraty et al., 2007). Given the observed synchronous trends of the PMR, PSR and R, it is evident that the PMR and PSR collectively demonstrate efficacy in quality control. In Fig. 21, the error-bar in purple shows the difference between the retrieved SID and buoys. The bias and standard deviation of the retrieved SID diminish as R, the PMR and the PSR increase, which indicates the effectiveness of these parameters for revealing the reliability of the result.

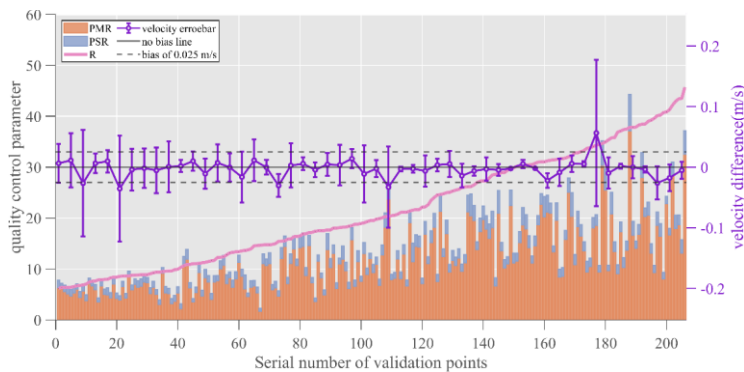


**Figure 21: Relationship between the velocity difference and quality control parameters.**

The coherence between the quality control parameters and the validation of the buoys is illustrated in Fig. 21, providing a foundation for the meticulous examination of the SID quality. As one of the main outlets of Arctic sea ice in the Atlantic Ocean, the sea ice concentration in the FS is inferior than the Arctic Basin (Peng and Meier, 2018; Wang et al., 2020), and the sea ice in the south and north of the strait render different morphologies in the images.

To investigate the quality of SID over the strait, we selected 80°N as the segmentation line and calculated the quality control parameters of SID in north and south of the segmentation line. The Fig. 22 shows the stacking bars of different parameters in different regions. For the sake of visualization, we normalize the PMR and PSR. The average values of these quality control parameters indicate that SID in the north of 80°N have higher quality. Comparison of quality control parameters for results with different time intervals reveals that the hours-level result possesses higher quality. Besides, the hours-level result also has greater mean value of quality control parameters in the south of 80°N where the sea ice is dispersive. High-concentration sea ice constrains the variability of sea ice motion and provides better spatial consistency, which is beneficial for retrieving SID. Similarly, the variability of the sea ice motion with short time interval is inconspicuous, providing a favorable scene for the algorithm. The sea ice kinematics in marginal ice zone are intricate, and the effects of wave on the fragmentary sea ice motion are evident (Williams et al., 2013, p.1), which increases the uncertainty of retrieval. The utilization of short time interval images for SID retrieval proves instrumental in enhancing the quality of monitoring sea ice motion within marginal ice zones.

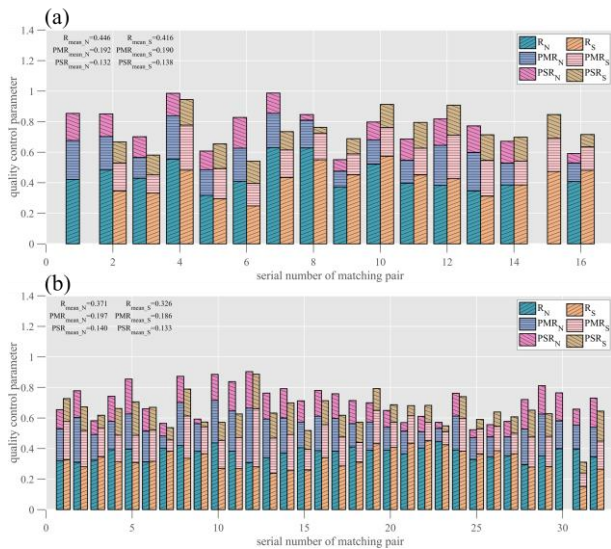


**Figure 22: Statistics of quality control parameters for individual retrieval SID. (a: hours-level, b: day-level). The suffix N and S mean north and south of 80°N in FS.**

## 2230 6 Conclusion

The retrieval of SID in FS is complicated due to the geographic specificity. Sea ice drift within the Arctic basin is dominated by two trends, the BG and TPD. The FS is the outlet of TPD as well as the intersection of the Atlantic and Arctic. The heavily fragmented sea ice in the strait, coupled with its fast velocity, significantly impacts the retrieval of SID. Our method, utilizing the multi-template matching and subpixel estimation approach for retrieving SID in FS, demonstrates great accuracy. We use 111 scenes of CZI images and obtain 48 sets of image pairs for analysis. The dataset is categorized into hours-level and day-level according to the time interval. We found that the day-level results are consistent with the CMEMS SID product, the hours-level results are slightly different from the CMEMS SID product due to the spatial and temporal variability of the sea ice motion. Validation is also conducted using IABP buoys. For the velocity, the bias of the day-level results and hours-level results with the buoys are -0.005 m/s and 0.000 m/s, respectively, and the RMSE of the day-level results and hours-level results with the buoys are 0.031 m/s and 0.036 m/s, respectively. For the flow direction, the bias of the day-level results and hours-level results with the buoys are 0.002 rad and 0.003 rad, respectively, and the RMSE of the day-level results and hours-level results with the buoys are 0.009 rad and 0.010 rad, respectively. The accuracy of the retrieved SID surpasses that of the SID products retrieved from AVHRR.

**Formatted:** Caption

**Formatted:** Font: (Asian) +Body Asian (宋体), (Asian) Chinese (Simplified, Mainland China)

**Deleted:** sea ice drift...ID in the ...S is complicated due to the geographic specificity of the region... Sea ice drift within the Arctic basin is dominated by two trends, the BG and TPD. The FS is the outlet of the ...PD as well as the intersection of the Atlantic and Arctic. The heavily fragmented nature of ...ea ice in this ...he strait, coupled with its fast motion...elocity, significantly impacts the accurate ...

**Deleted:** s...ng the multi-template matching and subpixel estimation approach to ...or retrieve ...etrieving SID in the ...S, produces...emonstrates a...greatpromising...result...accuracy.... We use 111 views ...enes of CZI images to ...nd obtain 48 sets of image pairs for analysis purposes... These images...dataset are ...s categorized into hours-level and day-level according to the time interval. We found that the day-level results...are consistent with the CMEMS SID product, the hours-level results...are ...s slightly different from the CMEMS SID product due to the spatial and temporal variability in

**Deleted:** carried out...onducted using IABP buoys. For the velocity, the bias values ...f the day-level results...and hours-level results...with the buoys are -0.0054...m/s and 0.000 m/s, respectively, and the RMSE values ...f the day-level results...and hours-level results...with the buoys are 0.027 ...31 m/s and 0.02...62...m/s, respectively. For the flow direction, the bias values ...f the day-level results...and hours-level results...with the buoys are 0.057 ...02 rad and 0.011 ...03 rad, respectively, and the RMSE values ...f the day-level results...and hours-level results...with the buoys are 0.313 ...09 rad and 0.631 ...10 rad, respectively. The accuracy of the retrieved SID surpasses that of the SID products obtained by

The method with multi-template matching and subpixel estimation for SID retrieval used in our study is an improvement of the traditional MCC algorithm. In our study, the reliability and accuracy of the algorithm are verified via comparison with the buoy. Additionally, the multi-template matching yields satisfactorily in terms of computational speed. Thus, we consider that our method for SID retrieval balances the computational cost and accuracy.

Our study verified the feasibility and validity of using CZI images for SID retrieval in FS. The spatial resolution of the retrieved SID is 4 km, which is much higher than the SID products based on scatterometers, radiometers and AVHRR. For our result, the spatial resolution is suitable for capturing complex sea ice motion in the FS. The SID products from scatterometers and radiometers, which possess broader coverage, are more suitable for the study of sea ice mass balance and assimilation of numerical prediction over the whole Arctic region. Our result also illustrates the high potential of the CZI for exploring the polar. At present, the HY-1C and HY-1D satellites are networked for observation, and the Chinese HY-1 series of satellites will be further utilized to advance polar research. Since 23 Dec 2021, the discontinuation of the Sentinel-1B satellite operation resulted in numerous data gaps in the CMEMS SID product, which severely limited the long-term sea ice motion study in FS. Through leveraging expansions of HY-1C data in future, we anticipate that SID retrieved from CZI will serve as the complement for the CMEMS SID product and facilitate the utilization of high spatial and temporal resolution product for sea ice dynamics research.

*Data availability.* The HY-1D data are available at <https://osdds.nsoas.org.cn/DataRetrieval>, provided by the NSOAS (last accessed on 26 December 2023). If you have not registered before, you will need to create an account to access the data. Then, you can enter your account and password to log in to the official website to access the HY-1D data. The sea ice drift product is available at [ftp://nrt.cmems-du.eu/Core/SEAICE\\_GLO\\_SEAICE\\_L4\\_NRT\\_OBSERVATIONS\\_011\\_006/DTU-GLO-SEAICE\\_DRIFT-NORTH-L4-NRT-OBS](ftp://nrt.cmems-du.eu/Core/SEAICE_GLO_SEAICE_L4_NRT_OBSERVATIONS_011_006/DTU-GLO-SEAICE_DRIFT-NORTH-L4-NRT-OBS), and the product was provided by the Copernicus Marine Service Information (CMEMS) (European Union-Copernicus Marine Service, 2015) (last accessed on 30 July 2023). The IABP buoy data are available at [https://iabp.apl.uw.edu/Data\\_Products/BUOY\\_DATA/FULL\\_RESOLUTION\\_DATA/Arctic/](https://iabp.apl.uw.edu/Data_Products/BUOY_DATA/FULL_RESOLUTION_DATA/Arctic/), provided by the International Arctic Buoy Programme.

*Author contributions.* Data curation, D.L. and L.S.; writing, D.L. and L.S.; methodology, D.L. L.S. J.L. T.Z. B.C. S.W. and M.W.; validation, D.L. T.Z. and S.W.; funding acquisition, L.S. and J.L. All authors have read and agreed to the published version of the paper. We dedicate this study to Prof Jianqiang Liu who sadly passed away in the line of work on 25 May 2023. He has played a key role in HY satellite technical configuration and made contributions during the preparation of this manuscript.

*Competing interests.* At least one of the (co-)authors is a member of the editorial board of *The Cryosphere*. The peer-review process was guided by an independent editor, and the authors also have no other competing interests to declare.

*Acknowledgments.* The authors would like to thank the editors and reviewers for their invaluable efforts in improving the paper. The authors would also like to thank the NSOAS, CMEMS, DTU and IABP for providing all the data needed for this paper. The authors would also like to thank GIV creators and PIVLAB crew for providing referential code.

**Deleted:** SID retrieval ...method with multi-template matching and subpixel estimation for SID retrieval used in our study is an improves ...improvement of the traditional MCC method...algorithm. In this ...ur study, the reliability and accuracy of the algorithm are verified by ...ia comparing ...omparison the results ...ith the buoy (...)

**Deleted:** in the application of the algorithm,...the method of ...ulti-template matching performs ...ields satisfactorily in terms of computational speed. Thus, we consider that the ...ur method used in this study (...)

**Deleted:** well (...)

**Deleted:** This ...ur study verifies ...erified the feasibility and validity of using CZI images for SID retrieval in the...FS. The spatial resolution of the retrieved SID is 4 km, which is much higher than that of the... SID products from ...ased on scatterometers, and other optical...VHRR. For our result, the spatial resolution sensors and...is suitable for capturing complex sea ice drift information...otion in the FS. T...e SID products from scatterometers and radiometers, which possessith...broader coverage, are more suitable for the study of sea ice mass balance and the assimilation...ssimilation of numerical prediction over the whole Arctic region. This ...ur result also illustrates the high potential of the CZI for sensor carried by China's HY-1D satellite over the polar regions...xploring the polar. At present, the HY-1C and HY-1D satellites have ...re been ...etworked for observation, and the Chinese HY-1 series of satellites will be further utilized to advance polar research. Since 23 Dec 2021, the Discontinuation ...iscontinuation of the Sentinel-1B satellite operation resulted in numerous data gaps on ...n the CMEMS SID products...from 2022 onwards ...hich severely limited the SID capacity to study ...ong-term sea ice drift ...otion study in the ...S. Through leveraging future ...xpansions of HY-1C data in future, we anticipate that CZI-retrieved ...ID retrieved from CZI will serve as the complement for thement...CMEMS SID products in forthcoming research..., ...nd facilitating ...acilitate the utilization of high spatial and resolution and high ...emporal resolution products...for studying (...)

**Deleted:** <https://osdds.nsoas.org.cn/>... provided by the NSOAS (last accessed on 30 ...6 July ...ecember 2023). If you have not registered before, you will need to create an account to access the data. Then, you can enter your account and password to log in to the official website to access the HY-1D data. The sea ice drift product is available at [ftp://nrt.cmems-du.eu/Core/SEAICE\\_GLO\\_SEAICE\\_L4\\_NRT\\_OBSERVATIONS\\_011\\_006/DTU-GLO-SEAICE\\_DRIFT-NORTH-L4-NRT-OBS](ftp://nrt.cmems-du.eu/Core/SEAICE_GLO_SEAICE_L4_NRT_OBSERVATIONS_011_006/DTU-GLO-SEAICE_DRIFT-NORTH-L4-NRT-OBS), and the product is (...)

**Deleted:** ... validation, D.L. T.Z. and S.W. (...)

*Financial support.* The research is funded by the National Key Research and Development Program of China (grant numbers 2021YFC2803300 and 2018YFC1407200), the Impact and Response of Antarctic Seas to Climate Change programme (grant number IRASCC2020-2022-No. 01-01-03), B.C was supported by the European Union's Horizon 2020 research and innovation framework programme (PolarRES project, grant number 101003590).

## References

- Aagaard, K. and Carmack, E. C.: The role of sea ice and other fresh water in the Arctic circulation, *Journal of Geophysical Research: Oceans*, 94, 14485–14498, <https://doi.org/10.1029/JC094iC10p14485>, 1989.
- Encyclopedia of Ocean Sciences: <http://www.sciencedirect.com:5070/referencework/9780128130827/encyclopedia-of-ocean-sciences>, last access: 13 December 2022.
- Arya, S. P. S.: Contribution of form drag on pressure ridges to the air stress on Arctic ice, *Journal of Geophysical Research* (1896-1977), 78, 7092–7099, <https://doi.org/10.1029/JC078i030p07092>, 1973.
- Arya, S. P. S.: A drag partition theory for determining the large-scale roughness parameter and wind stress on the Arctic pack ice, *Journal of Geophysical Research* (1896-1977), 80, 3447–3454, <https://doi.org/10.1029/JC080i024p03447>, 1975.
- Colony, R. and Thorndike, A. S.: An estimate of the mean field of Arctic sea ice motion, *J. Geophys. Res.*, 89, 10623, <https://doi.org/10.1029/JC089iC06p10623>, 1984.
- Cook, B. I., Smerdon, J. E., Seager, R., and Coats, S.: Global warming and 21st century drying, *Clim Dyn*, 43, 2607–2627, <https://doi.org/10.1007/s00382-014-2075-y>, 2014.
- Dethloff, K., Rinke, A., Benkel, A., Kølitzow, M., Sokolova, E., Kumar Saha, S., Handorf, D., Dorn, W., Rockel, B., von Storch, H., Haugen, J. E., Røed, L. P., Roeckner, E., Christensen, J. H., and Stendel, M.: A dynamical link between the Arctic and the global climate system, *Geophysical Research Letters*, 33, <https://doi.org/10.1029/2005GL025245>, 2006.
- Döscher, R., Vihma, T., and Maksimovich, E.: Recent advances in understanding the Arctic climate system state and change from a sea ice perspective: a review, *Atmospheric Chemistry and Physics*, 14, 13571–13600, <https://doi.org/10.5194/acp-14-13571-2014>, 2014.
- Dybkjaer, G.: Algorithm Theoretical Basis Document for OSI SAF Medium Resolution Sea Ice Drift Product, 2018.
- European Union-Copernicus Marine Service: Global Ocean - High Resolution SAR Sea Ice Drift, <https://doi.org/10.48670/MOI-00135>, 2015.
- Fang, Y., Wang, X., Li, G., Chen, Z., Hui, F., and Cheng, X.: Arctic sea ice drift fields extraction based on feature tracking to MODIS imagery, *International Journal of Applied Earth Observation and Geoinformation*, 120, 103353, <https://doi.org/10.1016/j.jag.2023.103353>, 2023.
- Farbman, Z., Fattal, R., Lischinski, D., and Szeliski, R.: Edge-preserving decompositions for multi-scale tone and detail manipulation, *ACM Trans. Graph.*, 27, 1–10, <https://doi.org/10.1145/1360612.1360666>, 2008.

Formatted: English (United Kingdom)

Formatted: Normal, Indent: First line: 0 cm

- Finnish Meteorological Institute, Rudels, B., and Carmack, E.: Arctic Ocean Water Mass Structure and Circulation, *Oceanog*, <https://doi.org/10.5670/oceanog.2022.116>, 2022.
- 2555 Girard-Ardhuin, F. and Ezraty, R.: Enhanced Arctic Sea Ice Drift Estimation Merging Radiometer and Scatterometer Data, *IEEE Trans. Geosci. Remote Sensing*, 50, 2639–2648, <https://doi.org/10.1109/TGRS.2012.2184124>, 2012.
- Gómez-Chova, L., Camps-Valls, G., Calpe, J., Guanter, L., and Moreno, J.: Cloud-screening algorithm for ENVISAT/MERIS multispectral images, *Geoscience and Remote Sensing, IEEE Transactions on*, 45, 4105–4118, <https://doi.org/10.1109/TGRS.2007.905312>, 2008.
- 2560 Haarpaintner, J.: Arctic-wide operational sea ice drift from enhanced-resolution QuikScat/SeaWinds scatterometry and its validation, *IEEE Trans. Geosci. Remote Sensing*, 44, 102–107, <https://doi.org/10.1109/TGRS.2005.859352>, 2006.
- Haine, T. W. N., Curry, B., Gerdes, R., Hansen, E., Karcher, M., Lee, C., Rudels, B., Spreen, G., de Steur, L., Stewart, K. D., and Woodgate, R.: Arctic freshwater export: Status, mechanisms, and prospects, *Global and Planetary Change*, 125, 13–35, <https://doi.org/10.1016/j.gloplacha.2014.11.013>, 2015.
- 2565 Hakkinen, S., Proshutinsky, A., and Ashik, I.: Sea ice drift in the Arctic since the 1950s, *Geophysical Research Letters*, 35, <https://doi.org/10.1029/2008GL034791>, 2008.
- Hollands, T. and Dierking, W.: Performance of a multiscale correlation algorithm for the estimation of sea-ice drift from SAR images: initial results, *Ann. Glaciol.*, 52, 311–317, <https://doi.org/10.3189/172756411795931462>, 2011.
- Hwang, B.: Inter-comparison of satellite sea ice motion with drifting buoy data, *International Journal of Remote Sensing*, 34, 8741–8763, <https://doi.org/10.1080/01431161.2013.848309>, 2013.
- 2570 Hyun, C.-U. and Kim, H.: A Feasibility Study of Sea Ice Motion and Deformation Measurements Using Multi-Sensor High-Resolution Optical Satellite Images, *Remote Sensing*, 9, 930, <https://doi.org/10.3390/rs9090930>, 2017.
- Johansson, A. M. and Berg, A.: Agreement and Complementarity of Sea Ice Drift Products, *IEEE J. Sel. Top. Appl. Earth Observations Remote Sensing*, 9, 369–380, <https://doi.org/10.1109/JSTARS.2015.2506786>, 2016.
- 2575 Kang, X., Gao, G., Hao, Q., and Li, S.: A Coarse-to-Fine Method for Cloud Detection in Remote Sensing Images, *IEEE Geoscience and Remote Sensing Letters*, PP, 1–5, <https://doi.org/10.1109/LGRS.2018.2866499>, 2018.
- Kruppen, T., Gerdes, R., Haas, C., Hendricks, S., Herber, A., Selyuzhenok, V., Smedsrud, L., and Spreen, G.: Recent summer sea ice thickness surveys in Fram Strait and associated ice volume fluxes, *The Cryosphere*, 10, 523–534, <https://doi.org/10.5194/tc-10-523-2016>, 2016.
- 2580 Krutsch, R. and Tenorio, D.: Histogram equalization, Freescale Semiconductor, Document Number AN4318, Application Note, 2011.
- Kwok, R.: Satellite remote sensing of sea-ice thickness and kinematics: a review, *Journal of Glaciology*, 56, 1129–1140, <https://doi.org/10.3189/002214311796406167>, 2010.
- Kwok, R., Schweiger, A., Rothrock, D. A., Pang, S., and Kottmeier, C.: Sea ice motion from satellite passive microwave imagery assessed with ERS SAR and buoy motions, *J. Geophys. Res.*, 103, 8191–8214, <https://doi.org/10.1029/97JC03334>, 1998.
- 2585

- Lavergne, T., Eastwood, S., Teffah, Z., Schyberg, H., and Breivik, L.-A.: Sea ice motion from low-resolution satellite sensors: An alternative method and its validation in the Arctic, *Journal of Geophysical Research: Oceans*, 115, <https://doi.org/10.1029/2009JC005958>, 2010.
- 590 Lei, R., Heil, P., Wang, J., Zhang, Z., Li, Q., and Li, N.: Characterization of sea-ice kinematic in the Arctic outflow region using buoy data, *Polar Research*, 35, 22658, <https://doi.org/10.3402/polar.v35.22658>, 2016.
- Li, X., Che, T., Li, X., Wang, L., Duan, A., Shangguan, D., Pan, X., Fang, M., and Bao, Q.: CASEarth Poles: Big Data for the Three Poles, *Bulletin of the American Meteorological Society*, 101, E1475–E1491, <https://doi.org/10.1175/BAMS-D-19-0280.1>, 2020.
- 595 Lopez-Acosta, R., Schodlok, M. P., and Wilhelmus, M. M.: Ice Floe Tracker: An algorithm to automatically retrieve Lagrangian trajectories via feature matching from moderate-resolution visual imagery, *Remote Sensing of Environment*, 234, 111406, <https://doi.org/10.1016/j.rse.2019.111406>, 2019.
- Lupton, R., Blanton, M. R., Fekete, G., Hogg, D. W., O’Mullane, W., Szalay, A., and Wherry, N.: Preparing Red-Green-Blue Images from CCD Data, *PASP*, 116, 133, <https://doi.org/10.1086/382245>, 2004.
- 600 Martin, T. and Augstein, E.: Large-scale drift of Arctic Sea ice retrieved from passive microwave satellite data, *J. Geophys. Res.*, 105, 8775–8788, <https://doi.org/10.1029/1999JC900270>, 2000.
- Maslanik, J., Stroeve, J., Fowler, C., and Emery, W.: Distribution and trends in Arctic sea ice age through spring 2011, *Geophysical Research Letters*, 38, <https://doi.org/10.1029/2011GL047735>, 2011.
- Pedersen, L. T., Saldo, R., and Fenger-Nielsen, R.: Sentinel-1 results: Sea ice operational monitoring, in: 2015 IEEE International Geoscience and Remote Sensing Symposium (IGARSS), 2015 IEEE International Geoscience and Remote Sensing Symposium (IGARSS), 2828–2831, <https://doi.org/10.1109/IGARSS.2015.7326403>, 2015.
- 605 Peng G. and Meier W. N.: Temporal and regional variability of Arctic sea-ice coverage from satellite data, *Annals of Glaciology*, 59, 191–200, <https://doi.org/10.1017/aog.2017.32>, 2018.
- Petrou, Z. I. and Tian, Y.: KARVONEN, *IEEE Transactions on Geoscience and Remote Sensing*, 55, 1339–1350, <https://doi.org/10.1109/TGRS.2016.2622714>, 2017.
- 610 Pizer, S. M., Amburn, E. P., Austin, J. D., Cromartie, R., Geselowitz, A., Greer, T., ter Haar Romeny, B., Zimmerman, J. B., and Zuiderveld, K.: Adaptive histogram equalization and its variations, *Computer Vision, Graphics, and Image Processing*, 39, 355–368, [https://doi.org/10.1016/S0734-189X\(87\)80186-X](https://doi.org/10.1016/S0734-189X(87)80186-X), 1987.
- Preller, R. H. and Posey, P. G.: A numerical model simulation of a summer reversal of the Beaufort Gyre, *Geophysical Research Letters*, 16, 69–72, <https://doi.org/10.1029/GL016i001p00069>, 1989.
- 615 Qiu, Y. and Li, X.-M.: Retrieval of sea ice drift from the central Arctic to the Fram Strait based on sequential Sentinel-1 SAR data, *IEEE Trans. Geosci. Remote Sensing*, 1–1, <https://doi.org/10.1109/TGRS.2022.3226223>, 2022.
- Reimnitz, E., Dethleff, D., and Nürnberg, D.: Contrasts in Arctic shelf sea-ice regimes and some implications: Beaufort Sea versus Laptev Sea, *Marine Geology*, 119, 215–225, [https://doi.org/10.1016/0025-3227\(94\)90182-1](https://doi.org/10.1016/0025-3227(94)90182-1), 1994.

- 620 Rigor, I. G., Clemente-Colon, P., and Hudson, E.: The international Arctic buoy programme (IABP): A cornerstone of the Arctic observing network, in: OCEANS 2008, OCEANS 2008, 1–3, <https://doi.org/10.1109/OCEANS.2008.5152136>, 2008.
- Robert Ezraty, Fanny Girard-Ardhuin, and Croizé-Fillon: Sea-Ice Drift in the Central Arctic Using the 89 GHz Brightness Temperatures of the Advanced Microwave Scanning Radiometer, 2007.
- Schwerdtfeger, P.: The Thermal Properties of Sea Ice, *Journal of Glaciology*, 4, 789–807, <https://doi.org/10.3189/S0022143000028379>, 1963.
- 625 Serreze, M. C., Barrett, A. P., Slater, A. G., Woodgate, R. A., Aagaard, K., Lammers, R. B., Steele, M., Moritz, R., Meredith, M., and Lee, C. M.: The large-scale freshwater cycle of the Arctic, *Journal of Geophysical Research: Oceans*, 111, <https://doi.org/10.1029/2005JC003424>, 2006.
- Serreze, M. C., Barrett, A. P., Stroeve, J. C., Kindig, D. N., and Holland, M. M.: The emergence of surface-based Arctic amplification, *The Cryosphere*, 3, 11–19, <https://doi.org/10.5194/tc-3-11-2009>, 2009.
- 630 Smedsrud, L. H., Halvorsen, M. H., Stroeve, J. C., Zhang, R., and Kloster, K.: Fram Strait sea ice export variability and September Arctic sea ice extent over the last 80 years, *The Cryosphere*, 11, 65–79, <https://doi.org/10.5194/tc-11-65-2017>, 2017.
- Stern, H. L. and Moritz, R. E.: Sea ice kinematics and surface properties from RADARSAT synthetic aperture radar during the SHEBA drift, *Journal of Geophysical Research: Oceans*, 107, SHE 14-1-SHE 14-10, <https://doi.org/10.1029/2000JC000472>, 2002.
- 635 Stow, D. A., Hope, A., McGuire, D., Verbyla, D., Gamon, J., Huemmrich, F., Houston, S., Racine, C., Sturm, M., Tape, K., Hinzman, L., Yoshikawa, K., Tweedie, C., Noyle, B., Silapaswan, C., Douglas, D., Griffith, B., Jia, G., Epstein, H., Walker, D., Daeschner, S., Petersen, A., Zhou, L., and Myneni, R.: Remote sensing of vegetation and land-cover change in Arctic Tundra Ecosystems, *Remote Sensing of Environment*, 89, 281–308, <https://doi.org/10.1016/j.rse.2003.10.018>, 2004.
- 640 Sumata, H., de Steur, L., Gerland, S., Divine, D. V., and Pavlova, O.: Unprecedented decline of Arctic sea ice outflow in 2018, *Nat Commun*, 13, 1747, <https://doi.org/10.1038/s41467-022-29470-7>, 2022.
- Sumata, H., de Steur, L., Divine, D. V., Granskog, M. A., and Gerland, S.: Regime shift in Arctic Ocean sea ice thickness, *Nature*, 615, 443–449, <https://doi.org/10.1038/s41586-022-05686-x>, 2023.
- Thielicke, W. and Stamhuis, E. J.: PIVlab – Towards User-friendly, Affordable and Accurate Digital Particle Image Velocimetry in MATLAB, *Journal of Open Research Software*, 2, <https://doi.org/10.5334/jors.bl>, 2014.
- 645 Torre, V. and Poggio, T. A.: On Edge Detection, *IEEE Transactions on Pattern Analysis and Machine Intelligence*, PAMI-8, 147–163, <https://doi.org/10.1109/TPAMI.1986.4767769>, 1986.
- Tsukernik, M., Deser, C., Alexander, M., and Tomas, R.: Atmospheric forcing of Fram Strait sea ice export: a closer look, *Clim Dyn*, 35, 1349–1360, <https://doi.org/10.1007/s00382-009-0647-z>, 2010.
- 650 Van Wyk de Vries, M. and Wickert, A. D.: Glacier Image Velocimetry: an open-source toolbox for easy and rapid calculation of high-resolution glacier velocity fields, *The Cryosphere*, 15, 2115–2132, <https://doi.org/10.5194/tc-15-2115-2021>, 2021.
- Wagner, T. J. W., Eisenman, I., and Mason, H. C.: How Sea Ice Drift Influences Sea Ice Area and Volume, *Geophysical Research Letters*, 48, e2021GL093069, <https://doi.org/10.1029/2021GL093069>, 2021.

- 2655 Wang, D.-Z., Wu, C.-H., Ip, A., Chan, C.-Y., and Wang, D.-W.: Fast Multi-template Matching Using a Particle Swarm Optimization Algorithm for PCB Inspection, in: Applications of Evolutionary Computing, Berlin, Heidelberg, 365–370, [https://doi.org/10.1007/978-3-540-78761-7\\_39](https://doi.org/10.1007/978-3-540-78761-7_39), 2008.
- Wang, M., König, M., and Oppelt, N.: Partial Shape Recognition for Sea Ice Motion Retrieval in the Marginal Ice Zone from Sentinel-1 and Sentinel-2, *Remote Sensing*, 13, 4473, <https://doi.org/10.3390/rs13214473>, 2021.
- Wang, X., Chen, R., Li, C., Chen, Z., Hui, F., and Cheng, X.: An Intercomparison of Satellite Derived Arctic Sea Ice Motion Products, *Remote Sensing*, 14, 1261, <https://doi.org/10.3390/rs14051261>, 2022.
- 2660 Wang, Z., Li, Z., Zeng, J., Liang, S., Zhang, P., Tang, F., Chen, S., and Ma, X.: Spatial and Temporal Variations of Arctic Sea Ice From 2002 to 2017, *Earth and Space Science*, 7, e2020EA001278, <https://doi.org/10.1029/2020EA001278>, 2020.
- Williams, T. D., Bennetts, L. G., Squire, V. A., Dumont, D., and Bertino, L.: Wave–ice interactions in the marginal ice zone. Part 1: Theoretical foundations, *Ocean Modelling*, 71, 81–91, <https://doi.org/10.1016/j.ocemod.2013.05.010>, 2013.
- 2665 Yan F., Xue W., ZhuoQi C., Gang L. I., FengMing H. U. I., and Xiao C.: Summer sea ice drift tracking and variation analysis in Fram Strait from 2011 to 2020, *Chinese Journal of Geophysics*, 66, 2726–2740, <https://doi.org/10.6038/cjg2022Q0025>, 2023.
- Zeng, T., Shi, L., Huang, L., Zhang, Y., Zhu, H., and Yang, X.: A Color Matching Method for Mosaic HY-1 Satellite Images in Antarctica, *Remote Sensing*, 15, 4399, <https://doi.org/10.3390/rs15184399>, 2023.
- 2670 Zu, Y., Lu, P., Leppäranta, M., Cheng, B., and Li, Z.: On the Form Drag Coefficient Under Ridged Ice: Laboratory Experiments and Numerical Simulations From Ideal Scaling to Deep Water, *Journal of Geophysical Research: Oceans*, 126, e2020JC016976, <https://doi.org/10.1029/2020JC016976>, 2021.
- Zuiderveld, K.: Contrast limited adaptive histogram equalization, in: *Graphics gems IV*, 474–485, 1994.